

HALL CURRENT AND ION SLIP IMPACT ON A  
OLDROYD-B NANOFLUID FLOW DRIVEN BY TWO  
CONCENTRIC ROTATING DISKS WITH  
CATTANEO-CHRISTOV HEAT FLUX



STUDENT NAME: HAFSA BINT E ARIF  
ENROLLMENT NO: 01-248202-004  
SUPERVISOR BY Prof. Dr. MUHAMMAD RAMZAN

A thesis submitted in fulfilment of the requirements for the award  
of degree of Masters of Science (Mathematics)

Department of Computer Science  
BAHRIA UNIVERSITY ISLAMABAD

Session (2020-2022)

## Approval of Examination

Scholar Name: Hafsa Bint E Arif

Registration Number: 71096

Enrollment: 01-248202-004

Program of Study: : MS (Mathematics)

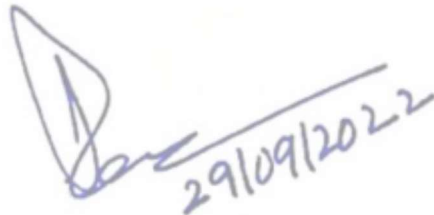
Thesis Title: Hall current and Ion slip impact on a Oldroyd-B nanofluid flow driven by two concentric rotating disks with Cattaneo-Christov heat flux.

It is to certify that the above scholar's thesis has been completed to my satisfaction and, to my belief, its standard is appropriate for submission for examination. I have also conducted plagiarism test of this thesis using HEC prescribed software and found similarity index 18% that is within the permissible limit set by the HEC for the MS/M. Phil degree thesis. I have also found the thesis in a format recognized by the BU for the MS/M. Phil thesis.

Supervisor Name: Prof. Dr. Muhammad Ramzan

Supervisor Signature:

Date:

A handwritten signature in blue ink, followed by the date 29/09/2022 written in blue ink.

## **Author's Declaration**

I, Hafsa Bint E Arif hereby state that my MS/MPhil thesis titled " Hall current and Ion slip impact on a Oldroyd-B nanofluid flow driven by two concentric rotating disks with Cattaneo-Christov heat flux " is my own work and has not been submitted previously by me for taking any degree from this university Bahria University or anywhere else in the country/world. At any time if my statement is found to be incorrect even after my Graduate the university has the right to withdraw/cancel my MS/MPhil degree

Name of Scholar: Hafsa Bint E Arif

Date: 15/9/2022

## Plagiarism Undertaking

I, solemnly declare that research work presented in the thesis titled” Hall current and Ion slip impact on a Oldroyd-B nanofluid flow driven by two concentric rotating disks with Cattaneo-Christov heat FLUX ” is solely my research work with no significant contribution from any other person. Small contribution / help wherever taken has been duly acknowledged and that complete thesis has been written by me.

I understand the zero tolerance policy of the HEC and Bahria University towards plagiarism. Therefore, I as an Author of the above titled thesis declare that no portion of my thesis has been plagiarized and any material used as reference is properly referred/ cited.

I undertake that if I am found guilty of any formal plagiarism in the above titled thesis even after award of MS/MPhil degree, the university reserves the right to withdraw / revoke my MS/MPhil degree and that HEC and the University has the right to publish my name on the HEC / University website on which names of students are placed who submitted plagiarized thesis.

Name of Scholar:Hafsa Bint E Arif

Date:15/09/2022

## Dedication

My respected supervisor, my parents, my husband, and my beloved son.

## Acknowledgements

Praise to be Almighty Allah, who is the Lord of the world, the Answer of prayers and the source of peace, whose blessing and exaltation flourished to the scared wealth of knowledge. Indeed, this difficult task was made possible with the help of Allah. Special praise and regards for his Last messenger, Holy Prophet Hazrat Muhammad (PBUH). Holy Prophet said that I AM the light, whoever follows ME, will never be in the darkness.

I feel great pleasure in expressing my profound and heartiest gratitude to my kind, devoted supervisor Dr. Muhammad Ramzan for his indispensable guidance, deep consideration, affection and active co-operation that made possible to this work to meet its end successfully well in time. Teachers like him are very precious assets for a nation who change the life of an individual and also nations. Such teachers make the density of a nation. I am proud that my supervisor is also one of the teachers and working with him is an honor for me.

I would also express my gratitude to all teachers. Due to their guidance and help am able to get the success of reaching my destination. The prominent among them are Dr. Jafar Husnain and Dr. Rizwan ul Haq who supported me in all course work as well as in the completion of this thesis. I like to thanks to all respected teachers at Department of Mathematics, Bahria University Islamabad Campus for providing us healthy academic environment.

My intense recognition is to my parents, and my husband who are always real pillar for my encouragement and showered their everlasting love, care and support throughout my life. Humble prayers, continuing support and encouragement of my family are always highly appreciated. I also appreciate the moral support of all my friends and PhD scholars especially Nazia shahmir who help me at every step and stage at my research work. Consequently, My all plea is to Allah the Almighty, the beneficent Whose blessings are always showered upon me via strengthening my wisdom and bestowed me with the knowledge of what he wants.

## **Abstract**

This study discusses the flow of Oldroyd-B nanofluid amidst two rotating disks with the inclusion of gyrotatic microorganisms. The stability of the nanofluid flow is strengthened by embedding the impact of the gyrotatic microorganisms. The Buongiorno model is adopted for the nanofluid flow. The Hall current and Ion slip impact are considered owing to the strong magnetic field taken perpendicular to the both disks. The envisioned model is tackled numerically and graphs of arising parameters are plotted against associated profiles. The physical quantities of interest are also investigated.

# TABLE OF CONTENTS

|  |            |
|--|------------|
| <b>AUTHOR’S DECLARATION</b>            | <b>ii</b>  |
| <b>PLAGIARISM UNDERTAKING</b>          | <b>iii</b> |
| <b>DEDICATION</b>                      | <b>iv</b>  |
| <b>ACKNOWLEDGEMENTS</b>                | <b>v</b>   |
| <b>ABSTRACT</b>                        | <b>vi</b>  |
| <b>LIST OF TABLES</b>                  | <b>xi</b>  |
| <b>LIST OF FIGURES</b>                 | <b>xii</b> |
| <b>LIST OF SYMBOLS</b>                 | <b>xv</b>  |
| <b>1 INTRODUCTION</b>                  | <b>4</b>   |
| 1.1 Basic preliminaries and laws ..... | 4          |
| 1.2 Fluid.....                         | 4          |
| 1.3 Fluid mechanics.....               | 4          |
| 1.3.1 Fluid statics.....               | 4          |
| 1.3.2 Fluid dynamics.....              | 5          |
| 1.4 Nanofluid.....                     | 5          |
| 1.5 Stress.....                        | 5          |
| 1.5.1 Shear stress.....                | 5          |
| 1.5.2 Normal stress.....               | 5          |
| 1.6 Strain.....                        | 5          |



|        |                                       |    |
|--------|---------------------------------------|----|
| 1.7    | Flow.....                             | 6  |
| 1.7.1  | Laminar flow.....                     | 6  |
| 1.7.2  | Turbulent flow.....                   | 6  |
| 1.8    | Viscosity.....                        | 6  |
| 1.8.1  | Dynamic viscosity ( $\mu$ ).....      | 6  |
| 1.8.2  | Kinematic viscosity ( $\nu$ ).....    | 6  |
| 1.9    | Newton's viscosity law.....           | 7  |
| 1.10   | Newtonian fluids.....                 | 7  |
| 1.11   | Non-Newtonian fluids.....             | 7  |
| 1.12   | Density.....                          | 8  |
| 1.13   | Pressure.....                         | 8  |
| 1.14   | Magnetohydrodynamics (MHD).....       | 8  |
| 1.15   | Heat flux.....                        | 8  |
| 1.16   | Hall current.....                     | 9  |
| 1.17   | Gyrotactic microorganism.....         | 9  |
| 1.18   | Mechanism of heat transfer.....       | 9  |
| 1.18.1 | Conduction.....                       | 9  |
| 1.18.2 | Convection.....                       | 10 |
| 1.18.3 | Radiation.....                        | 10 |
| 1.19   | Convective boundary conditions.....   | 10 |
| 1.20   | Fundamental laws.....                 | 11 |
| 1.20.1 | Mass conservation law.....            | 11 |
| 1.20.2 | The conservation of momentum law..... | 11 |

|          |                                   |           |
|----------|-----------------------------------|-----------|
| 1.20.3   | Law of energy conservation.....   | 12        |
| 1.21     | Concentration.....                | 12        |
| 1.22     | Thermal diffusivity.....          | 12        |
| 1.23     | Thermal conductivity.....         | 13        |
| 1.24     | Maxwell fluid Model.....          | 13        |
| 1.25     | Oldroyd-B fluid Model.....        | 15        |
| 1.26     | Dimensionless numbers.....        | 16        |
| 1.26.1   | Reynolds number.....              | 16        |
| 1.26.2   | Prandtl Number .....              | 17        |
| 1.26.3   | Coefficient of skin friction..... | 17        |
| 1.26.4   | Nusselt number.....               | 17        |
| 1.26.5   | Biot number.....                  | 18        |
| 1.26.6   | Thermophoresis parameter.....     | 18        |
| 1.26.7   | Brownian motion parameter.....    | 18        |
| 1.26.8   | Schmidt number.....               | 19        |
| 1.26.9   | Peclet number.....                | 19        |
| 1.26.10  | Lewis number.....                 | 19        |
| 1.26.11  | Sherwood number.....              | 20        |
| <b>2</b> | <b>LITERATURE REVIEW</b>          | <b>21</b> |
| 2.1      | Introduction.....                 | 21        |
| 2.2      | Literature review.....            | 23        |

|          |  |           |
|----------|--|-----------|
| <b>3</b> | <b>MHD SWIRLING FLOW AND HEAT TRANSFER IN MAXWELL FLUID DRIVEN BY TWO COAXIALLY ROTATING DISKS WITH VARIABLE THERMAL CONDUCTIVITY</b>    | <b>27</b> |
| 3.1      | Mathematical formulation .....   | 28        |
| 3.2      | Nusselt Number .....   | 32        |
| 3.3      | Numerical Solution.....  | 35        |
| 3.4      | Discussion.....  | 36        |
| <b>4</b> | <b>HALL CURRENT AND ION SLIP IMPACT ON A OLDROYD-B NANOFUID DRIVEN BY TWO CONCENTRIC ROTATING DISKS WITH CATTANEO-CHRISTOV HEAT FLUX</b> | <b>50</b> |
| 4.1      | Mathematical modeling.....   | 51        |
| 4.2      | Important physical quantiesty.....   | 57        |
| 4.3      | Numerical approach.....  | 58        |
| 4.4      | Discussion.....  | 59        |
| <b>5</b> | <b>CONCLUSIONS AND FUTURE WORK</b>   | <b>68</b> |
| 5.1      | Chapter 3.....   | 68        |
| 5.2      | Chapter 4.....   | 69        |
| 5.3      | Future work.....   | 70        |
|          | <b>REFERENCES</b>  | <b>71</b> |

## LIST OF TABLES

| <b>Table No.</b> | <b>Caption</b>   | <b>Page No</b> |
|------------------|--|----------------|
| Table 3.1        | Comparison table of $\theta'(0)$ from previous publication                       | 33             |
| Table 3.2        | Numerical values of Nusselt number for various parameters                        | 34             |
| Table 3.3        | Comparison table of $f''(0)$ , $g'(0)$ , and $\Lambda$ from previous publication | 35             |
| Table 4.1        | Numerical values of Nusselt number, Sherwood number, and motile microorganism    | 67             |

## LIST OF FIGURES

| <b>Figure No.</b> | <b>Caption</b>   | <b>Page No.</b> |
|-------------------|--|-----------------|
| Figure 3.1        | Geometry of the problem                                    | 30              |
| Figure 3.2(a)     | Influence of $S_2$ on $f(\eta)$ , when<br>$S_1 = 0$        | 38              |
| Figure 3.2(b)     | Influence of $S_2$ on $f'(\eta)$ , when<br>$S_1 = 0$       | 39              |
| Figure 3.2(c)     | Influence of $S_2$ on $g(\eta)$ , when<br>$S_1 = 0$        | 39              |
| Figure 3.2(d)     | Influence of $S_2$ on $\theta(\eta)$ , when<br>$S_1 = 0$   | 40              |
| Figure 3.3(a)     | Influence of $S_2$ on $f(\eta)$ , when<br>$S_1 = 0.5$      | 40              |
| Figure 3.3(b)     | Influence of $S_2$ on $f'(\eta)$ , when<br>$S_1 = 0.5$     | 41              |
| Figure 3.3(c)     | Influence of $S_2$ on $g(\eta)$ , when<br>$S_1 = 0.5$      | 41              |
| Figure 3.3(d)     | Influence of $S_2$ on $\theta(\eta)$ , when<br>$S_1 = 0.5$ | 42              |
| Figure 3.4(a)     | Influence of $M$ on $f(\eta)$                              | 42              |

|               |  |    |
|---------------|--|----|
| Figure 3.4(b) | Influence of $M$ on $f'(\eta)$               | 43 |
| Figure 3.4(c) | Influence of $M$ on $g(\eta)$                | 43 |
| Figure 3.4(d) | Influence of $M$ on $\theta(\eta)$           | 44 |
| Figure 3.5(a) | Influence of $Re$ on $f(\eta)$               | 44 |
| Figure 3.5(b) | Influence of $Re$ on $g(\eta)$               | 45 |
| Figure 3.5(c) | Influence of $Re$ on $\theta(\eta)$          | 45 |
| Figure 3.6(a) | Influence of $\beta_1$ on $f(\eta)$          | 46 |
| Figure 3.6(b) | Influence of $\beta_1$ on $f'(\eta)$         | 46 |
| Figure 3.6(c) | Influence of $\beta_1$ on $g(\eta)$          | 47 |
| Figure 3.6(d) | Influence of $\beta_1$ on $\theta(\eta)$     | 47 |
| Figure 3.7(a) | Influence of $\varepsilon$ on $\theta(\eta)$ | 48 |
| Figure 3.7(b) | Influence of $Pr$ on $\theta(\eta)$          | 48 |
| Figure 3.8(a) | Influence of $M$ on $P(\eta)$                | 49 |
| Figure 3.8(b) | Influence of $S_2$ on $P(\eta)$              | 49 |
| Figure 4.1    | Geometry of the problem                      | 52 |
| Figure 4.2    | Influence of $\beta_1$ on $f'(\eta)$         | 61 |
| Figure 4.3    | Influence of $\beta_2$ on $f'(\eta)$         | 61 |
| Figure 4.4    | Influence of $\beta_1$ on $g(\eta)$          | 62 |
| Figure 4.5    | Influence of $\beta_2$ on $g(\eta)$          | 62 |
| Figure 4.6    | Influence of $N_b$ on $\theta(\eta)$         | 63 |
| Figure 4.7    | Influence of $Pr$ on $\theta(\eta)$          | 63 |
| Figure 4.8    | Influence of $\beta_{1l}$ on $\theta(\eta)$  | 64 |

|             |   |    |
|-------------|---|----|
| Figure 4.9  | Influence of $\beta_{i2}$ on $\theta(\eta)$ | 64 |
| Figure 4.10 | Influence of $Le$ on $\phi(\eta)$           | 65 |
| Figure 4.11 | Influence of $N_t$ on $\phi(\eta)$          | 65 |
| Figure 4.12 | Influence of $Pe$ on $h(\eta)$              | 66 |
| Figure 4.13 | Influence of $Sc$ on $h(\eta)$              | 66 |
| Figure 4.14 | Influence of $Le$ on $h(\eta)$              | 67 |

## LIST OF SYMBOLS

### Symbols

---

|              |                                    |
|--------------|------------------------------------|
| $u, v, w$    | Velocity components                |
| $r, \phi, z$ | Cylindrical coordinates            |
| $B_0$        | Magnetic field                     |
| $\mu$        | Dynamic viscosity                  |
| $\nu$        | Kinematic viscosity                |
| $\lambda_1$  | Relaxation time                    |
| $\lambda_2$  | Retardation time                   |
| $T$          | Temperature                        |
| $T_1$        | Temperature of lower disk          |
| $T_2$        | Temperature of upper disk          |
| $\alpha^*$   | Thermal diffusivity                |
| $K$          | Thermal conductivity               |
| $C_p$        | Specific heat capacity             |
| $C$          | Nano particle concentration        |
| $C_1$        | Concentration of lower disk        |
| $C_2$        | Concentration of upper disk        |
| $N$          | Motile microorganism               |
| $N_1$        | Motile microorganism of lower disk |
| $N_2$        | Motile microorganism of upper disk |
| $Re$         | Reynold number                     |



|                          |  |
|--------------------------|--|
| $Pr$                     | Prandtl number                                 |
| $M$                      | Magnetic parameter                             |
| $\beta_1$                | Deborah number of relaxation time parameter    |
| $\beta_2$                | Deborah number of retardation time parameter   |
| $D_T$                    | Thermophoretic diffusion coefficient           |
| $D_B$                    | Brownian diffusion coefficient                 |
| $Sc$                     | Schmidt number                                 |
| $Le$                     | Lewis number                                   |
| $Pe$                     | Peclet number                                  |
| $S_1, S_2$               | Stretching parameters of lower and upper disks |
| $\Omega$                 | Rotational parameter                           |
| $N_t$                    | Thermophoretic parameter                       |
| $N_b$                    | Brownian motion parameter                      |
| $\Lambda$                | Pressure gradient parameter                    |
| $\beta_{i1}, \beta_{i2}$ | Biot numbers                                   |
| $\Omega^*$               | Difference of motile microorganism pressure    |
| $P$                      | pressure                                       |
| $\alpha$                 | Hall current parameter                         |
| $\beta_h$                | Ion-slip parameter                             |
| $D_n$                    | Microorganisms diffusion                       |
| $B$                      | Chemotactic constant                           |
| $W_c$                    | Maximum cell swimming speed                    |
| $\varepsilon$            | Pressure parameter                             |
| $q_w$                    | Wall heat flux                                 |

|                    |                                   |
|--------------------|-----------------------------------|
| $q_m$              | Wall mass flux                    |
| $q_n$              | Wall motile microorganism flux    |
| $\gamma$           | thermal relaxation time           |
| $\lambda$          | thermal relaxation time parameter |
| $\sigma$           | Electrical conductivity           |
| $Nu_{r1}, Nu_{r2}$ | Nusselt numbers                   |
| $Sh_{r1}, Sh_{r2}$ | Sherwood numbers                  |
| $Nn_{r1}, Nn_{r2}$ | motile microorganisms fluxes      |
| $f(\eta)$          | axial velocity                    |
| $f'(\eta)$         | Radial velocity                   |
| $g(\eta)$          | Azimuthal velocity                |
| $\theta(\eta)$     | Temperature profile               |
| $\phi(\eta)$       | Concentration profile             |
| $h(\eta)$          | motile microorganism profile      |
| $\eta$             | Similarity variable               |
| $d$                | Distance between two disks        |

# Chapter 1

## INTRODUCTION

### 1.1 Basic preliminaries and laws

This chapter includes some basic definitions, concepts, and laws that will help in understanding the works in the next two chapters.

### 1.2 Fluid

A material that can flow and deforms continuously when subjected to shear stress. Fluids include mercury, cooking oil, blood, and oxygen.

### 1.3 Fluid mechanics

It is the branch of science that studies the fluid behaviour whether they are moving or at rest. Fluid can be divided into two branches as follows:

#### 1.3.1 Fluid statics

Fluid statics is a field of fluid mechanics that deals with fluids that aren't moving relative to one another.

### 1.3.2 Fluid dynamics

Fluid dynamics is a branch of fluid mechanics concerned with the properties of liquids in motion.

## 1.4 Nanofluid

A nanofluid is a liquid that contains nanometer-sized particles known as nanoparticles. Nanotubes, metals, and oxides are common nanoparticles found in nanofluids. Water ( $H_2O$ ), ethylene glycol ( $C_2H_6O_2$ ), and oil are the most prevalent basic fluids.

## 1.5 Stress

Stress is defined as the force per unit area within the deformed body. Symbolically, We have

$$Stress = \frac{Restoring\ force}{Area\ of\ the\ material}.$$

In the SI system, the dimension is  $\left[\frac{M}{LT^2}\right]$  and the unit of stress is  $kg/m.s^2$ . It is divided into two categories.

### 1.5.1 Shear stress

Shear stress occurs when an external force operates parallel to the surface unit area.

### 1.5.2 Normal stress

Normal stress is the type of stress that occurs when a force operates vertically against a surface of unit area.

## 1.6 Strain

Strain is a dimensionless quantity that is used to quantify an object deformation when a force is applied to it.

## 1.7 Flow

Flow is defined as a material that deforms easily and fluently in the presence of various types of forces. Flow is further subdivided into two primary subcategories, which are as follows:

### 1.7.1 Laminar flow

Laminar flow occurs when fluid moves in regular channels with no interruption between layers.

### 1.7.2 Turbulent flow

Turbulent flow occurs when the fluid particles in the flow field have an uneven velocity.

## 1.8 Viscosity

The viscosity of a fluid is a fundamental feature that characterizes the fluid resistance to flow when many forces impact on it. There are two ways to describe the viscosity.

### 1.8.1 Dynamic viscosity ( $\mu$ )

It is the fluid characteristic that determines the fluid resistance to any deformation caused by the applied forces. The dynamic viscosity is also known as absolute viscosity. Mathematically, this may be expressed as follows:

$$\mu = \tau * \frac{dy}{du}. \quad (1.1)$$

Its dimension is  $ML^{-1}T^{-1}$  and its SI unit is  $Kg/m.s$ .

### 1.8.2 Kinematic viscosity ( $\nu$ )

It is the ratio of absolute viscosity and density with the fact that both have same temperature.

Mathematically it is represented by

$$\nu = \frac{\mu}{\rho}. \quad (1.2)$$

Its SI unit is  $m^2/s$  and its dimension is  $\left[\frac{L^2}{T}\right]$ .

## 1.9 Newton's viscosity law

Newton's law of viscosity defines the relationship between shear stress and shear rate in a fluid subjected to mechanical stress. Mathematically it can be represented as follows:

$$\tau_{yx} \propto \frac{du}{dy}, \quad (1.3)$$

or

$$\tau_{yx} = \mu \left( \frac{du}{dy} \right), \quad (1.4)$$

where  $\tau_{yx}$  denotes the shear force applied to the fluid's element,  $\mu$  denotes the proportionality constant and  $\frac{du}{dy}$  denotes the velocity gradient.

## 1.10 Newtonian fluids

These are the fluids that obey Newton's law of viscosity and have a constant viscosity. Shear force ( $\tau_{yx}$ ) in these fluids is related linearly to the gradient of velocity ( $\frac{du}{dy}$ ). Newtonian fluids include alcohol, water, glycerine, and kerosene oil.

## 1.11 Non-Newtonian fluids

The Newton's law of viscosity does not apply to these fluids. Shear stress ( $\tau_{yx}$ ) and velocity gradient have a nonlinear and direct connection here. Non-Newtonian fluids include toothpaste, butter, fabric paint etc. It is represented as:

$$\tau_{yx} \propto \left( \frac{du}{dy} \right)^n, \quad n \neq 1, \quad (1.5)$$

or

$$\tau_{yx} = k \frac{du}{dy}, \quad k = m \left( \frac{du}{dy} \right)^{n-1}, \quad (1.6)$$

where  $k$  the apparent viscosity,  $n$  the flow behaviour index and  $m$  the consistency index. For  $n = 1$  Eq. (1.6) converts to Newton's law of viscosity.

## 1.12 Density

Density is defined as the mass of a substance per unit volume. It is stated as follows:

$$\rho = \frac{m}{V}. \quad (1.7)$$

The SI unit of density is  $kg/m^3$  with dimension  $ML^{-3}$ .

## 1.13 Pressure

Pressure is defined as the force exerted per unit area on a surface. The pressure can be expressed mathematically as:

$$P = \frac{F}{A}. \quad (1.8)$$

The SI unit of pressure is  $N/m^2$ .

## 1.14 Magnetohydrodynamics (MHD)

Magnetohydrodynamics (MHD) is the study of electrically conducting fluid dynamics. The name magnetohydrodynamics is derived from the terms magneto which means magnetic field, hydro means liquid, and dynamic means movement. Such fluids include plasmas, liquids, metals, and salt water.

## 1.15 Heat flux

Heat flux is the flow of energy per unit area and time. The heat flow is a measurement of the energy transfer produced by temperature, which leads to the temperature balance among substance. Mathematically it can be expressed as:

$$\mathbf{q} = -k(\nabla T), \quad (1.9)$$

in which  $\mathbf{q}$  is heat flux,  $k$  represent material conductivity and  $\nabla T$  represent temperature gradient. Its SI unit is  $W/sq.m^2$ .

## 1.16 Hall current

When an electrical current passes through a sample in the presence of a magnetic field, a potential proportionate to the current and magnetic field arises across the material in a direction perpendicular to both the current and the magnetic field. This is known as Hall current. Edwin Hall, who discovered the phenomenon in 1897, is commemorated with this effect's name.

## 1.17 Gyrotactic microorganism

These are motile microorganisms found in lakes, rivers, and seas. Gyrotactic microorganisms are utilised in experiments because they aid in bio-convective movement. When a significant number of microorganisms congregate on the upper layer of suspension, the layer becomes thick, and the microorganisms become unstable and begin to move downward, resulting in bio-convective phenomenon.

## 1.18 Mechanism of heat transfer

Heat is a type of energy that moves from a warmer to a colder place. Heat transfer occurs when two things of different temperatures come into contact with each other. Heat is dispersed by three basic mechanisms: conduction, convection, and radiation.

### 1.18.1 Conduction

It is the phenomenon by which heat is transferred from a hot location to a cold part of a liquid or solid by collisions of free electrons and molecules. This event does not involve the transfer of molecules. Mathematically,

$$\mathbf{q} = -kA\nabla T, \tag{1.10}$$



or

$$\mathbf{q} = -kA \frac{dT}{dx}, \quad (1.11)$$

where  $\mathbf{q}$  denotes the heat flow  $A$  is the surface area,  $k$  is the thermal conductivity,  $(\frac{dT}{dx})$  shows the temperature gradient, and the negative sign refers that heat is transmitted from high to low temperature.

### 1.18.2 Convection

Convection occurs when a heated fluid, like as air or water, is pushed to move away from the source of heat, bringing energy with it.

$$\mathbf{q} = -HA(\nabla T). \quad (1.12)$$

Here,  $H$  stands for convective heat transfer coefficient,  $\nabla T$  for temperature difference between surface and fluid,  $A$  stands for area.

### 1.18.3 Radiation

Radiation is the transfer of energy from one medium to another in the form of waves or particles. The radiation stefan-boltzmann law governs radiation.

$$\mathbf{q} = e\sigma A(\Delta T)^4, \quad (1.13)$$

where  $\mathbf{q}$  is depicted as transfer of heat,  $e$  is the system emissivity,  $\sigma$  is the Stephen-Boltzmann constant, area is denoted by  $A$ , and  $(\Delta T)^4$  is the difference of temperature between two systems to the fourth power.

## 1.19 Convective boundary conditions

Convective boundary conditions are also known as Robin boundary conditions at times. This type of circumstance is frequently defined on a wall. These are stated mathematically as:

$$k \left( \frac{\partial T}{\partial m_i} \right)_{x_i} = h [T_f(x_i, t) - T_w(x_i, t)]. \quad (1.14)$$

This equation states that condition equals convection. Here  $h$  is the heat transfer coefficient,  $x_i$  is the location at the boundary,  $T_f$  is the fluid temperature, and  $T_w$  is the wall temperature.

## 1.20 Fundamental laws

The fundamental laws that are used for the flow specification in the subsequential analysis are given below.

### 1.20.1 Mass conservation law

The conservation of mass states that a body mass remains constant while it is moving. It sometimes referred to as the continuity equation. Mathematically,

$$\frac{D\rho}{Dt} + \rho \nabla \cdot \mathbf{V} = 0, \quad (1.15)$$

or

$$\frac{\partial \rho}{\partial t} + (\mathbf{V} \cdot \nabla) \rho + \rho \nabla \cdot \mathbf{V} = 0, \quad (1.16)$$

or

$$\frac{\partial \rho}{\partial t} + \nabla \cdot (\rho \mathbf{V}) = 0, \quad (1.17)$$

where density is depicted by  $\rho$ ,  $\frac{\partial \rho}{\partial t}$  is time derivatives,  $\mathbf{V}$  represents the fluid velocity. It is known as the equation of continuity. For the steady flow Eq. (1.17) becomes

$$\nabla \cdot (\rho \mathbf{V}) = 0, \quad (1.18)$$

and if the fluid is incompressible then Eq. (1.18) implies that

$$\nabla \cdot \mathbf{V} = 0. \quad (1.19)$$

### 1.20.2 The conservation of momentum law

The total linear momentum of a closed system is said to be constant. Generally it is given by

$$\rho \frac{D\mathbf{V}}{Dt} = \text{div } \boldsymbol{\tau} + \rho \mathbf{b}, \quad (1.20)$$

where  $\boldsymbol{\tau} = -\mathbf{p}\mathbf{I} + \mathbf{S}$ , denotes the Cauchy stress tensor,  $\rho \left(\frac{D\mathbf{V}}{Dt}\right)$  is represents internal force, and  $\rho \mathbf{b}$  ia a body force.

### 1.20.3 Law of energy conservation

Law of conservation of energy is also known as energy equation and is given by

$$\rho C_p \frac{DT}{Dt} = \boldsymbol{\tau} \cdot \mathbf{L} - \nabla \cdot \mathbf{q} + \rho r, \quad (1.21)$$

in which  $\mathbf{q}$  for heat flux vector and  $r$  for thermal radiation. Energy equation without thermal radiation takes the form

$$\rho C_p \frac{DT}{Dt} = \boldsymbol{\tau} \cdot \mathbf{L} + k \nabla^2 T, \quad (1.22)$$

where  $\mathbf{q} = -k \nabla T$ ,  $\mathbf{L} = \nabla \mathbf{V}$ ,  $k$  denotes the thermal conductivity and  $T$  for temperature.

## 1.21 Concentration

For nanoparticle, the volume fraction equation is:

$$\frac{\partial C}{\partial t} + \mathbf{V} \cdot \nabla C = -\frac{1}{\rho_p} \nabla \cdot \mathbf{j}_p, \quad (1.23)$$

$$\mathbf{j}_p = -\rho_p D_B \nabla C - \rho_p D_T \frac{\nabla T}{T_\infty}, \quad (1.24)$$

$$\frac{\partial C}{\partial t} + \mathbf{V} \cdot \nabla C = D_B \nabla^2 C + D_T \frac{\nabla^2 T}{T_\infty}. \quad (1.25)$$

Here,  $C$  is nanoparticle concentration,  $T$  is fluid temperature,  $T_\infty$  is the ambient temperature,  $D_B$  stands for Brownian diffusion,  $D_T$  for thermophoretic coefficient.

## 1.22 Thermal diffusivity

Thermal diffusivity is a material specific property for describing the unsteady conductive heat flow. This value describes how speedily a material respond to change in temperature. It is the relationship between thermal conductivity and the product of specific heat capacity and density. Mathematically it can be written as:

$$\alpha = \frac{k}{\rho C_p}, \quad (1.26)$$

where  $k$  indicates the thermal conductivity,  $C_p$  the specific heat capacity and  $\rho$  the density.

## 1.23 Thermal conductivity

The measurement of the ability of a material to conduct heat is defined as thermal conductivity. According to Fourier Law of heat conduction, it is defined as “The amount of heat transfer rate ( $Q$ ) through a material of unit thickness ( $L$ ) times unit cross section area ( $A$ ) and unit temperature difference ( $\Delta T$ )”. Mathematically written as:

$$k = \frac{QL}{A(\Delta T)}, \quad (1.27)$$

in SI system thermal conductivity has unit  $\frac{W}{m.K}$  and dimension is  $(\frac{ML}{T^3\theta})$ .

## 1.24 Maxwell fluid Model

The momentum equation for Maxwell fluid is

$$\rho(\mathbf{V} \cdot \nabla) \mathbf{V} = -\nabla p + \nabla \cdot \mathbf{S} + \mathbf{J} \times \mathbf{B}, \quad (1.28)$$

where

$$\mathbf{J} = \sigma(\mathbf{V} \times \mathbf{B}), \quad \mathbf{B} = [0, 0, B_0], \quad (1.29)$$

The Maxwell liquid extra stress tensor  $\mathbf{S}$  is written as:

$$\left(1 + \lambda_1 \frac{D}{Dt}\right) \mathbf{S} = \mathbf{S} + \lambda_1 \frac{D\mathbf{S}}{Dt} = \mu \mathbf{A}_1, \quad (1.30)$$

where  $\lambda_1$  denotes relaxation time,  $\frac{D}{Dt}$  for the distinction of covariant variables,  $\mathbf{A}_1$  stands for the first Rivlin-Erickson tensor and  $\mu$  stands for dynamic viscosity. The first tensor of Rivlin-Erickson is

$$\mathbf{A}_1 = \text{grad } \mathbf{V} + (\text{grad } \mathbf{V})^t, \quad (1.31)$$

in which  $t$  is the matrix transpose for 3-D flow, we get

$$\begin{aligned} \mathbf{A}_1 &= \begin{bmatrix} \frac{\partial u_r}{\partial r} & \frac{\partial u_\theta}{\partial r} & \frac{\partial u_z}{\partial r} \\ \frac{1}{r} \frac{\partial u_r}{\partial \theta} - \frac{u_\theta}{r} & \frac{1}{r} \frac{\partial u_\theta}{\partial \theta} + \frac{u_r}{r} & \frac{1}{r} \frac{\partial u_z}{\partial \theta} \\ \frac{\partial u_r}{\partial z} & \frac{\partial u_\theta}{\partial z} & \frac{\partial u_z}{\partial z} \end{bmatrix} + \begin{bmatrix} \frac{\partial u_r}{\partial r} & \frac{\partial u_\theta}{\partial r} & \frac{\partial u_z}{\partial r} \\ \frac{1}{r} \frac{\partial u_r}{\partial \theta} - \frac{u_\theta}{r} & \frac{1}{r} \frac{\partial u_\theta}{\partial \theta} + \frac{u_r}{r} & \frac{1}{r} \frac{\partial u_z}{\partial \theta} \\ \frac{\partial u_r}{\partial z} & \frac{\partial u_\theta}{\partial z} & \frac{\partial u_z}{\partial z} \end{bmatrix}^t \\ \mathbf{A}_1 &= \begin{bmatrix} 2\frac{\partial u_r}{\partial r} & \frac{\partial u_\theta}{\partial r} + \frac{1}{r} \frac{\partial u_r}{\partial \theta} - \frac{u_\theta}{r} & \frac{\partial u_z}{\partial r} + \frac{\partial u_r}{\partial z} \\ \frac{\partial u_\theta}{\partial r} + \frac{1}{r} \frac{\partial u_r}{\partial \theta} - \frac{u_\theta}{r} & 2\left(\frac{1}{r} \frac{\partial u_\theta}{\partial \theta} + \frac{u_r}{r}\right) & \frac{1}{r} \frac{\partial u_z}{\partial \theta} + \frac{\partial u_\theta}{\partial z} \\ \frac{\partial u_r}{\partial z} + \frac{\partial u_z}{\partial r} & \frac{\partial u_\theta}{\partial z} + \frac{1}{r} \frac{\partial u_z}{\partial \theta} & 2\frac{\partial u_z}{\partial z} \end{bmatrix}, \end{aligned} \quad (1.32)$$

for  $\mathbf{S}$  tensor of rank two, we have

$$\frac{D\mathbf{S}}{Dt} = \frac{\partial \mathbf{S}}{\partial t} + (\nabla \cdot \mathbf{V}) \mathbf{S} - \mathbf{S}\mathbf{L} - \mathbf{S}\mathbf{L}^t, \quad (1.33)$$

where  $\mathbf{L} = \text{grad} \mathbf{V}$

applying the operator  $1 + \lambda_1 \frac{D}{Dt}$  on law of momentum conservation. In the absence of body force, we obtain the expression,

$$\rho \left(1 + \lambda_1 \frac{D}{Dt}\right) \frac{\partial \mathbf{V}}{\partial t} = - \left(1 + \lambda_1 \frac{D}{Dt}\right) \nabla p + \left(1 + \lambda_1 \frac{D}{Dt}\right) (\nabla \cdot \mathbf{S}), \quad (1.34)$$

by using

$$\frac{D}{Dt}(\nabla) = \nabla \cdot \left(\frac{D}{Dt}\right), \quad (1.35)$$

applying the Eqs. (1.35) in (1.28), we obtain

$$\rho \left(1 + \lambda_1 \frac{D}{Dt}\right) \frac{\partial \mathbf{V}}{\partial t} = - \left(1 + \lambda_1 \frac{D}{Dt}\right) \nabla_p + \mu \cdot (\nabla \cdot \mathbf{A}_1) + \left(1 + \lambda_1 \frac{D}{Dt}\right) (\mathbf{J} \times \mathbf{B}), \quad (1.36)$$

in the absence of pressure gradient, the above Eq. (1.36) becomes

$$\rho \left(1 + \lambda_1 \frac{D}{Dt}\right) \frac{\partial \mathbf{V}}{\partial t} = \mu \cdot (\nabla \cdot \mathbf{A}_1) + \left(1 + \lambda_1 \frac{D}{Dt}\right) (\mathbf{J} \times \mathbf{B}), \quad (1.37)$$

For steady Maxwell liquid flow in cylindrical coordinates is expressed as:

$$\begin{aligned} u_r \frac{\partial u_r}{\partial r} + \frac{u_\theta}{r} \frac{\partial u_r}{\partial \theta} + u_z \frac{\partial u_r}{\partial z} - \frac{v_\theta^2}{r} &= -\frac{1}{\rho} \left( \frac{\partial p}{\partial r} \right) + \nu \left[ \begin{aligned} &\frac{1}{\partial r} \left( \frac{1}{r} \frac{\partial}{\partial r} (r u_r) + \frac{1}{r^2} \frac{\partial^2 u_r}{\partial \theta^2} \right) \\ &- \frac{2}{r^2} \frac{\partial u_\theta}{\partial \theta} + \frac{\partial^2 u_r}{\partial z^2} \end{aligned} \right] \\ &- \lambda_1 \left[ \begin{aligned} &u_r^2 \frac{\partial^2 u_r}{\partial r^2} + u_z^2 \frac{\partial^2 u_r}{\partial z^2} + 2u_r u_z \frac{\partial^2 u_r}{\partial r \partial z} - \frac{2u_r u_\theta}{r} \frac{\partial u_\theta}{\partial r} \\ &- \frac{2u_\theta u_z}{r} \frac{\partial u_\theta}{\partial z} + \frac{u_r u_\theta^2}{r^2} + \frac{u_\theta^2}{r} \frac{\partial u_r}{\partial r} \end{aligned} \right], \end{aligned} \quad (1.38)$$

$$\begin{aligned} u_r \frac{\partial u_\theta}{\partial r} + \frac{u_\theta}{r} \frac{\partial u_\theta}{\partial \theta} + u_z \frac{\partial u_\theta}{\partial z} - \frac{u_r u_\theta}{r} &= -\frac{1}{\rho} \left( \frac{\partial p}{\partial \theta} \right) + \nu \left[ \begin{aligned} &\frac{1}{\partial r} \left( \frac{1}{r} \frac{\partial}{\partial r} (r u_\theta) + \frac{1}{r^2} \frac{\partial^2 u_\theta}{\partial \theta^2} \right) \\ &- \frac{2}{r^2} \frac{\partial u_r}{\partial \theta} + \frac{\partial^2 u_\theta}{\partial z^2} \end{aligned} \right] \\ &- \lambda_1 \left[ \begin{aligned} &u_r^2 \frac{\partial^2 u_\theta}{\partial r^2} + u_z^2 \frac{\partial^2 u_\theta}{\partial z^2} + 2u_r u_z \frac{\partial^2 u_\theta}{\partial r \partial z} + \frac{2u_r u_\theta}{r} \frac{\partial u_r}{\partial r} \\ &+ \frac{2u_\theta u_z}{r} \frac{\partial u_r}{\partial z} - \frac{2u_r^2 u_\theta}{r^2} - \frac{u_\theta^2}{r} \frac{\partial u_\theta}{\partial r} + \frac{u_\theta^3}{r^2} \end{aligned} \right], \end{aligned} \quad (1.39)$$

$$\begin{aligned} u_r \frac{\partial u_z}{\partial r} + \frac{u_\theta}{r} \frac{\partial u_z}{\partial \theta} + u_z \frac{\partial u_\theta}{\partial z} &= -\frac{1}{\rho} \left( \frac{\partial p}{\partial z} \right) + \nu \left( \frac{1}{\partial r} \left( \frac{1}{r} \frac{\partial u_z}{\partial r} \right) + \frac{1}{r^2} \frac{\partial^2 u_z}{\partial \theta^2} + \frac{\partial^2 u_z}{\partial z^2} \right) \\ &- \lambda_1 \left( u_r^2 \frac{\partial^2 u_z}{\partial r^2} + 2u_r u_z \frac{\partial^2 u_z}{\partial r \partial z} + u_z^2 \frac{\partial^2 u_z}{\partial z^2} + \frac{u_\theta^2}{r^2} \frac{\partial u_z}{\partial r} \right). \end{aligned} \quad (1.40)$$

## 1.25 Oldroyd-B fluid Model

We investigate an Oldroyd-B fluid flow caused by a rotating disk. The Oldroyd-B fluid model stress tensor is expressed as:

$$\left(1 + \lambda_1 \frac{D}{Dt}\right) \mathbf{S} = \mu \left(1 + \lambda_2 \frac{D}{Dt}\right) \mathbf{A}_1, \quad (1.41)$$

where  $\lambda_1$ ,  $\lambda_2$ ,  $\mu$ ,  $\mathbf{S}$  are the relaxation and retardation times, the dynamic viscosity and extra stress tensor respectively. The following are the mathematical relationships for mass and momentum conservation in an incompressible MHD fluid flow:

$$\nabla \cdot \mathbf{V} = 0, \quad (1.42)$$

$$\rho \mathbf{a} = -\nabla p + \nabla \cdot \mathbf{S} + \mathbf{J} \times \mathbf{B}, \quad (1.43)$$

for the velocity vector  $\mathbf{V}$  the material time derivative is shown by  $\mathbf{a}$ .

$$\mathbf{a} = \frac{d\mathbf{V}}{dt} = \frac{\partial \mathbf{V}}{\partial t} + (\mathbf{V} \cdot \nabla) \mathbf{V}, \quad (1.44)$$

the density of the fluid is depicted by  $\rho$  and  $p$  denotes for the fluid pressure, employing divergence on the Eq. (1.41), we get

$$\left(1 + \lambda_1 \frac{D}{Dt}\right) \nabla \cdot \mathbf{S} = \mu \left(1 + \lambda_2 \frac{D}{Dt}\right) \nabla \cdot \mathbf{A}_1, \quad (1.45)$$

after applying the operator  $\left(1 + \lambda_1 \frac{D}{Dt}\right)$  on Eq. (1.43) and utilizing the result of Eq. (1.45), we have

$$\rho \left(1 + \lambda_1 \frac{D}{Dt}\right) \mathbf{a} = -\left(1 + \lambda_1 \frac{D}{Dt}\right) \nabla p + \mu \left(1 + \lambda_2 \frac{D}{Dt}\right) \nabla \cdot \mathbf{A}_1 + \left(1 + \lambda_1 \frac{D}{Dt}\right) (\mathbf{J} \times \mathbf{B}), \quad (1.46)$$

where  $\mathbf{A}_1 = \nabla \mathbf{V} + (\nabla \mathbf{V})^t$  is the first Rivlin-Ericksen tensor and  $\frac{D}{Dt}$  the upper convective derivative. The axisymmetric three-dimensional steady flow is:

$$\mathbf{V} = [u(r, \varphi, z), v(r, \varphi, z), w(r, \varphi, z)]. \quad (1.47)$$

## 1.26 Dimensionless numbers

### 1.26.1 Reynolds number

It is the most essential dimensionless number used to distinguish between different flow characteristics such as laminar and turbulent flow. It represents the ratio of inertial to viscous forces. Laminar flow occurs at low Reynolds numbers, when viscous forces dominate. Turbulent flow occurs at high Reynolds numbers, where inertial forces dominate. The Reynolds number is used to distinguish between distinct flow regimes within a comparable fluid, such as laminar or turbulent flow. It may be stated mathematically as:

$$\text{Re} = \frac{\textit{Inertial force}}{\textit{Viscous force}},$$
$$\text{Re} = \frac{vL}{\nu}. \quad (1.48)$$

Here,  $v$  signifies fluid velocity,  $L$  means characteristic length, and  $\nu$  denotes kinematic viscosity.

### 1.26.2 Prandtl Number

The Prandtl number is the relationship between momentum and thermal diffusivity. It is dimensionless number. The Prandtl number is employed in heat transfer to govern the thicknesses of momentum and thermal boundary layers. Mathematically it can be expressed by

$$\text{Pr} = \frac{\nu}{\alpha} = \frac{\mu C_p}{k}, \quad (1.49)$$

where  $\mu$  signifies dynamic viscosity,  $C_p$  denotes specific heat, and  $k$  denotes thermal conductivity.

### 1.26.3 Coefficient of skin friction

Skin friction occurs when fluid runs across a surface and creates a certain degree of drag. It occurs when a fluid collides with the surface of a solid, causing the fluid's velocity to



slow. The skin friction coefficient is defined as

$$C_f = \frac{\tau_w}{\frac{1}{2}\rho U_w^2}, \quad (1.50)$$

in which  $\tau_w$  for wall shear stress,  $\rho$  is for density and  $U_w$  represents the free stream velocity.

#### 1.26.4 Nusselt number

It is a dimensionless quantity that measures the ratio of convective to conductive heat transfer. Mathematically

$$Nu_L = \frac{h\Delta T}{k\Delta T/L} = \frac{hL}{k}, \quad (1.51)$$

where  $h$  stands for convective heat transfer,  $L$  for characteristic length and  $k$  for thermal conductivity of the fluid.

#### 1.26.5 Biot number

It is defined as the internal conductive resistance divided by the external convection resistance. Mathematically:

$$Bi = \frac{\text{Internal conductive resistance}}{\text{External convective resistance}},$$
$$Bi = \frac{h}{k}L, \quad (1.52)$$

where  $L$  is the characteristic length, thermal conductivity of the body is denoted by  $k$ , and  $h$  shows the convective heat transfer coefficient.

#### 1.26.6 Thermophoresis parameter

Thermophoresis is a method that is used to prevent the mixing of dissimilar particles owing to a pressure differential as they travel together or to separate the particles after they have mixed. Thermophoresis is positive on a cold surface and negative on a hot surface. It may be stated mathematically as:

$$N_t = \frac{(\rho C)_p D_T (T_f - T_\infty)}{(\rho C_p)_f \nu T_\infty}, \quad (1.53)$$

where  $T_f$  and  $T_\infty$  are the wall temperature and ambient temperature,  $D_T$  is thermophoretic diffusion coefficient and  $\nu$  the kinematic viscosity.

### 1.26.7 Brownian motion parameter

Brownian motion occurs due to size of the nanoparticles in a nanofluid. It is a nanoscale mechanism that displays the thermal influences of nanofluid. Mathematically

$$N_b = \frac{\tau D_B (C_f - C_\infty)}{\nu}, \quad (1.54)$$

$$\tau = \frac{(\rho C)_p}{(\rho C_p)_f}. \quad (1.55)$$

In the above equation  $\tau$  is the ratio of effective heat and heat capacity of the nanoparticles and fluid respectively,  $\nu$  the Kinematic viscosity.  $C_f$  the walls concentration,  $C_\infty$  the ambient concentration and  $D_B$  the brownian diffusion coefficient.

### 1.26.8 Schmidt number

Schmidt number  $Sc$  is defined as the dimensionless quantity which measures the ratio of momentum diffusivity (viscosity) to mass diffusivity. It is introduced by Heinrich Wilhelm Schmidt in (1892-1972). Mathematically,

$$Sc = \frac{\nu}{D_B}, \quad (1.56)$$

where  $\nu$  is kinematic viscosity and  $D_B$  is mass diffusivity.

### 1.26.9 Peclet number

The ratio of heat flow rates between conduction and convection for a uniform temperature gradient is known as the Peclet number. The Peclet number is the dimensionless number denoted by  $Pe$ . Jean Claude Eugène Péclet, a French scientist, is honoured by its name.

$$Pe = \frac{Lu}{\alpha}, \quad (1.57)$$

where  $L$  is the Characteristic length,  $u$  is fluid velocity, and  $\alpha$  is the thermal diffusivity.

### 1.26.10 Lewis number

The ratio between thermal diffusivity to mass diffusivity is called Lewis number. It is dimensionless number denoted by  $Le$ . Mathematically,

$$Le = \frac{\alpha}{D}, \quad (1.58)$$

where  $\alpha$  denotes thermal diffusivity, and  $D$  shows mass diffusivity.

Lewis number can also be expressed as:

$$Le = \frac{Sc}{Pr}. \quad (1.59)$$

### 1.26.11 Sherwood number

The ratio of convective mass transfer to mass diffusivity is known as the Sherwood number. Sherwood numbers shows the effectiveness of mass convection at the surface. Sherwood number  $Sc$  is the dimensionless number. Mathematically it can be written as,

$$Sc = \frac{\text{Convective mass transfer}}{\text{Mass diffusion rate}},$$

$$Sc = \frac{k_m}{D/L}, \quad (1.60)$$

where  $k_m$  is the convective mass transfer coefficient,  $L$  is a characteristic length,  $D$  is the mass diffusivity.

## Chapter 2

# LITERATURE REVIEW

### 2.1 Introduction

A nanofluid is a fluid that includes nanoparticles (particles with a diameter of less than 100nm) inserted in the base fluid. Carbon nanotubes, metals, and oxides are commonly employed as nanoparticles. Common base fluids are water, ethylene glycol, and oil. Nanofluid differs from other base fluids in that the nanomaterials are emersed in the base fluids. These particles are introduced into base fluids to enhance thermal conductivity and heat transmission. These are used to attain the maximum enhancement in thermal properties at lower concentrations. Nanoliquids have the potential to improve heat transfer rates in a diverse range of applications, such as nuclear reactors, industrial cooling applications, transportation, micro-electromechanical system, chemical catalytic reactors, and blood flow in the cardiovascular system engaging the Navier-Stokes equation. The need for nanofluids as coolants in automobiles takes into account their tiny size, which means they use less energy to regulate road resistance. There have been a lot of studies on nanofluids improved heat transfer capabilities, particularly thermal conductivity.

The concept of nanofluids has been studied using three different types of models, including the single phase model, the Eulerian-Eulerian multi-phase mixture model, and the Eulerian-Lagrangian discrete phase model. The most popular model is the single phase model, which is predicated on the idea that nanofluids behave like regular fluids. The other two phase models are considered in the interaction between fluid and solid particles. The Eulerian-Lagrangian

discrete phase model contains two independent phases. The first is the solid phase, and the second is the fluid phase. While the Eulerian-Eulerian multi-phase mixture model creates the fluid-solid mixture.

Non-Newtonian liquid flows are important in a variety of industrial and technical operations, such as paper manufacture, petroleum drilling, glass blowing, the expulsion of polymeric liquids and melts, paints and so far. Non-Newtonian liquids are materials in which shear stress and velocity gradient do not have a direct or linear relationship. As a result, academicians have proposed a variety of non-Newtonian fluid mathematical models according to their application requirements. In polymer processing, rate-type fluid models such as Maxwell, Oldroyd-B, or Burgers fluids are commonly used to predict stress relaxation. Maxwell fluids and viscoelastic fluids, have a wide range of industrial use, such as glass blowing, polymer sheet extrusion, plastic film manufacture, hot rolling, crystal growth, and so on. Maxwell liquid is the least complicated non-Newtonian liquid subclass among these models. The Oldroyd-B fluid is a non-Newtonian visco-elastic fluid that represents the stress-relaxation relationship. This model is a modification of the Maxwell fluid with the addition of time retardation. The Oldroyd-B fluid is a fascinating and helpful nonlinear model that allows researchers to investigate significant relaxation and retardation characteristics. Many researchers employed the Oldroyd-B fluid model in many situations due to its significant qualities. Unlike many polymeric materials, the Oldroyd-B model cannot represent shear thinning or thickening. The Oldroyd-B fluid analyzes the flow relaxation and retardation time characteristics.

The study of electrically conducting fluid motion in the existence of a magnetic field is known as Magnetohydrodynamics (MHD). Whereas magneto means magnetic field, hydro means fluids, and dynamics mean forces. An electromotive force is produced by the relative motion of a conducting fluid and a magnetic field, and that motion produces electrical currents. The fundamental idea of MHD is that a magnetic field may produce current in conductive fluids. There are countless uses for magnetohydrodynamics (MHD), including the analysis of the Ionosphere, the creation of the Earth's magnetic field, and the use of electromagnetic forces to pump liquid metals. Many researchers have drawn their attention to this kind of flow because of its multiple uses in technological problems such as MHD generators, nuclear reactors, geothermal energy extraction, and MHD generators. Hydromagnetic methods are also utilized

to separate non-metallic inclusions from molten metals. The MHD depends upon the order of density  $\sigma(w \times B)$ , where  $\sigma$  means electrical conductivity,  $w$  for the velocity field, and  $\mathbf{B}$  is the magnetic field. Because of this fact, the fluid produces flow along magnetic field lines because the current creates an additional induced magnetic field.

## 2.2 Literature review

In a variety of systems, nanofluids have shown enormous heat transfer capabilities. Nanofluids are used in medicine delivery, power generation, micromanufacturing processes, metallurgical industries, and thermal treatment. Initially, thermal energy and heat transmission were carried out using basic fluids with modest heat conductivity, such as water, oil, and heat transfer. In 1995, with the advancement of nanostructures, Choi and Eastman [1] worked for the first time on nanofluid, considering it for cooling and coolant purposes in technologies. They observed that nanofluids had greater conduction and heat transfer rate efficiency gain than simple or basic liquids used in previous experiments. Many researchers worked on nanofluids using the concept of Choi's idea, some of them are [2, 3]. Ramzan et al. [4] deliberated a 3D nanofluid thin film moving at a constant velocity via heat radiation and across a tilted rotating disk. Dogonchi and Ganji [5] studied the Cattaneo-Christov heat flux and thermal radiation for an unstable contracting MHD flow. They evaluated the heat transport of the nanofluid between two plates. Udawattha et al. [6] scrutinized the effective viscosity of nanofluids based on suspended nanoparticles. Hussanan et al. [7] investigated the use of Oxide nanoparticles for energy augmentation in engine nanofluids and base fluid. Salari et al. [8] investigated nanofluids to enhance the wall heat transfer rate and minimize the time for food processing in the industry. Many researchers are looking at some recent experiments involving heat and mass transfer using nanofluids [9 – 13].

Non-Newtonian fluids have a wide range of uses in different fields. Shampoos, blood at low shear rates, soaps, apple sauce, and other non-Newtonian fluids can be found in everyday life. The characteristics of all non-Newtonian fluids can't be fully explained by any specific single relation. As a result, academicians have proposed several mathematical models for non-Newtonian fluids. Maxwell constitutive equations are the simplest rate-type fluids and have

relaxation time characteristics. Maxwell [14] was the first to present the Maxwell model theory to explain viscoelastic behavior. Bodnar et al. [15] used the Johnson-Segalman equation to obtain the constitutive equation of Maxwell fluids, which is the rheological equation of state. For investigating boundary layer issues in fluid dynamics researchers prefer to use the Maxwell fluid model. Reynardy and Wang [16] have examined significant boundary layer properties in Maxwell fluid flows. A study of MHD in Maxwell fluid flows near vertical surfaces with thermophoresis and chemical reaction may be found in [17]. Maxwell fluid flow with changing thermal conductivity is demonstrated by Mustafa et al. [18]. Hayat et al. [19] investigated Maxwell nanofluid radiative flow over a heated stretched surface. A few researchers [20 – 24] have investigated the Maxwell fluid models in different phenomena.

The Oldroyd-B liquid is also a form of non-Newtonian liquid. The relaxation and retardation times of Oldroyd-B fluid are inspired. This model is an expansion of the Maxwell fluid model with the inclusion of time retardation. Oldroyd-B [25] was used to test the fluid model. Irfan et al. [26] investigated the magnetic field and chemical reaction properties of Oldroyd-B nanofluid flow in a stretched cylinder. Khan et al. [27] explored the flow of Oldroyd-B nanofluid with motile microorganisms. Abbas et al. [28] investigated thin film analysis for time-dependent Oldroyd-B fluids using a rotating disk. Hafeez et al. [29] examined the radiation of Oldroyd-B fluid flow across a revolving disk. In the existence of time-dependent MHD, Anwar et al. [30] studied the flow of Oldroyd-B fluid with thermal radiation and heat source-sink. Ye [31] focused on the global regularity of the Oldroyd-B model in high dimensions. Ersoy [32] examined the magnetohydrodynamics flow of the Oldroyd-B fluid across two infinite rotating disks traveling with a uniform angular velocity. The flow of an Oldroyd-B fluid confined across the two infinite coaxial parallel spinning disks was numerically modeled by Bhatnagar and Perera [33]. Sajid et al. [34] proposed a model in which an Oldroyd-B model boundary layer flow in the area of stagnation point over a stretched sheet. Some researchers worked on the Oldroyd-B model in different areas [35 – 38].

The heat transport phenomenon of a revolving disk has become an intriguing study subject. This is because it is used in specialized applications like turbine systems, jet engines, food processing, circulations of the atmosphere, and so on. Pearson [39] investigate the viscous flow between (two) spinning disks and determined that the majority of the fluid revolves faster than

either of the two disks. The Newtonian flow between (two) spinning disks was investigated by Arora and Stokes [40]. They discovered that increasing Reynold number causes stronger heat transmission when disks rotate in different directions and reduced heat transfer when disks rotate in the same way. Turkeyilmazoglu [41] investigated fluid flow over an impermeable spinning disk that was moving upward/downward. Turkeyilmazoglu [42] also investigated a steady flow by a spinning disk and discovered that the existence of radial electric parameters (positive or negative) had a significant impact on flow and thermal boundary layer. Khan et al. [43] investigated bioconvective flow using a variety of conditions, including a magnetic field. They noticed an improvement in axial velocity as the Reynolds number increased. In their recent research on the numerical investigation of fluid flow heat transfer characteristics. Bilal et al. [44] employed different numerical approaches to resolve the transmuted equations. Several researchers [45 – 50] investigated alternative nanofluid flows between (two) rotating disks afterward.

MHD is the study of the behavior, impact, and characteristics of a magnetic field over viscous fluids. Magneto fluids include salt water, plasmas, and electrolytes. It would be useful to explore the effect of a magnetic field on fluid flow. Alfén [51] was the first to invent the field of MHD. He was awarded the Nobel Prize in Physics in 1970 for his contributions to the field of MHD. Rashidi et al. [52] investigated the significant uses of MHD in peristaltic flow, pulsatile flow, simple flow, and drug administration. Hsu [53] studied the unsteady Couette flow with heat transfer between two parallel plates in an inclined magnetic field. Along with a uniform horizontal magnetic field, Turkeyilmazoglu and M. [54] studied the flow and transfer of heat on a rotating disk. Hayes [55] investigated the Stokes issue with a vertical plate in a rotating frame in the presence of a magnetic field. Devi et al. [56] investigated heat radiation impact on MHD flow on a nonporous spinning disk. Abbas et al. [57] developed a numerical solution for nanoparticles in various base fluids with slip and MHD effect. Khatsayuk et al. [58] investigated the numerical modeling of MHD vortex technology, and its verification is also provided.

Gyrotactic microorganisms enhance the mass transfer, which occurs in micro volumes, microscale mixing, and stability of nanofluid. The concept of bioconvection was initially proposed by Platt [59]. More information about gyrotactic bacteria was later supplied by Kessler



[60]. Basha and Sivaraj [61] examined blood flow numerically using several non-Newtonian fluid models in the circulatory system with gyrotactic microorganisms. Hussain et. al [62] observed the squeezing MHD bio-thermal convection flow of a micropolar nanofluid between two parallel disks with multiple slip effects. Li et al. [63] investigated the unstable mixed bioconvection flow of a nanofluid between two spinning disks that were either contracting or expanding. Shehzad et al. [64] studied the effect of double-diffusive Cattaneo-Christov theory on the Maxwell nanofluid bioconvection on isolated spinning disks. Zuhra et al. [65] noticed the gyrotactic nanoparticles and microorganisms together with second-grade nanofluid flow and heat transfer in which fluid temperature rises against the thermophoresis parameter.

## Chapter 3

# MHD SWIRLING FLOW AND HEAT TRANSFER IN MAXWELL FLUID DRIVEN BY TWO COAXIALLY ROTATING DISKS WITH VARIABLE THERMAL CONDUCTIVITY

MHD flow of Maxwell fluid between two coaxially parallel spinning disks is considered in this chapter. Disks are rotating with different angular velocities in the same direction. The pressure and heat transfer study is performed while accounting for the effects of an axial magnetic field and thermal conductivity that varies with temperature. Von Kármán similarity approach employed to transform the momentum and energy equations into nonlinear ODEs. The enriched flow model is numerically solved using MATLAB bvp4c scheme. The disks notably alter the classical flow pattern occurring between the disks, which is one of the key physical implications of this work. The observations revealed that as the Reynolds number upsurges, the pressure field dwindled near the lower disk. The thermal conductivity characteristic plays

an important role in increasing fluid temperature.

### 3.1 Mathematical formulation

The axisymmetric Maxwell fluid flow is considered when it is contained between two coaxially spinning parallel disks that are stretched linearly. The lower disk rotates with angular velocity  $\Omega_1$  while the upper disk spins with angular velocity  $\Omega_2$  at a fixed distance. For the mathematical representation, the cylindrical coordinates  $(r, \varphi, z)$  is used. Let  $s_1$  and  $s_2$  represent the lower and upper disk stretching ratios, accordingly. The fluid temperatures at the bottom and upper disks are considered to be  $T_1$  and  $T_2$ , accordingly. Corresponding to the  $z$ -axis, a homogeneous magnetic field of magnitude  $B_0$  is applied. The basic equations for the Maxwell fluid model for continuity, momentum, and energy equations are shown:

The continuity equation is

$$\nabla \cdot \mathbf{V} = 0. \quad (3.1)$$

The momentum equation is

$$\rho(\mathbf{V} \cdot \nabla) \mathbf{V} = -\nabla p + \nabla \cdot \mathbf{S} + \mathbf{J} \times \mathbf{B}, \quad (3.2)$$

where  $\mathbf{V}$  shows the velocity vector,  $p$  denotes the fluid pressure,  $\rho$  is the fluid density,  $\mathbf{J}$  is the current density with the electrical conductivity  $\sigma$ ,  $\mathbf{B}$  shows the magnetic field, and  $\mathbf{S}$  is the extra stress tensor for Maxwell fluid are all represented by

$$\mathbf{J} = \sigma(\mathbf{V} \times \mathbf{B}), \quad \mathbf{B} = [0, 0, B_0],$$

$$\mathbf{S} + \lambda_1 \frac{D\mathbf{S}}{Dt} = \mu \mathbf{A}_1, \quad (3.3)$$

where

$$\mathbf{A}_1 = \mathbf{L} + \mathbf{L}^t.$$

The dynamic viscosity is  $\mu$ , the relaxation time is denoted by  $\lambda_1$ , the first Rivlin Erickson tensor

is  $\mathbf{A}_1$ , and  $\frac{D}{Dt}$  is the contravariant convected derivative.

$$\frac{D\mathbf{S}}{Dt} = \frac{\partial\mathbf{S}}{\partial t} + (\mathbf{V}\cdot\nabla)\mathbf{S} - \mathbf{L}\mathbf{S} - \mathbf{S}\mathbf{L}^t, \quad (3.4)$$

where

$$\mathbf{L} = \text{grad } \mathbf{V},$$

applying divergence on both sides of Eq. (3.3)

$$\left(1 + \lambda_1 \frac{D}{Dt}\right) \mathbf{S} = \mu \nabla \cdot \mathbf{A}_1, \quad (3.5)$$

operating  $1 + \lambda_1 \frac{D}{Dt}$  on both sides of Eq. (3.2), we get

$$\left(1 + \lambda_1 \frac{D}{Dt}\right) \left(\rho \frac{d\mathbf{V}}{dt} + \nabla p\right) = \mu \nabla \cdot \mathbf{A}_1 + \left(1 + \lambda_1 \frac{D}{Dt}\right) (\mathbf{J} \times \mathbf{B}). \quad (3.6)$$

The energy equation is:

$$\rho C_p (\mathbf{V}\cdot\nabla) T = -\nabla \cdot \mathbf{q}, \quad (3.7)$$

where  $T$  denotes fluid temperature and  $\mathbf{q}$  denotes heat flow and is given as:

$$\mathbf{q} = -k(T)\nabla T, \quad (3.8)$$

The velocity field  $\mathbf{V}$  for axisymmetric steady flow is

$$\mathbf{V} = [u(r, z), v(r, z), w(r, z)]. \quad (3.9)$$

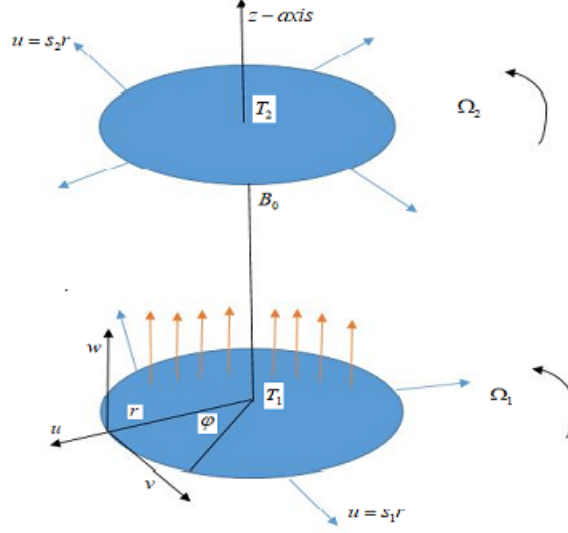


Fig 3.1 Geometry of the Problem

In components form, Eqs. (3.1), (3.2), and (3.7) can be expressed as:

$$\frac{\partial(ru)}{\partial r} + \frac{\partial(rw)}{\partial z} = 0, \quad (3.10)$$

$$\begin{aligned} u \frac{\partial u}{\partial r} + w \frac{\partial u}{\partial z} - \frac{v^2}{r} = & -\frac{1}{\rho} \frac{\partial p}{\partial r} + \nu \left( 2 \frac{\partial^2 u}{\partial r^2} + \frac{\partial^2 u}{\partial z^2} + \frac{\partial^2 w}{\partial r \partial z} + \frac{2}{r} \frac{\partial u}{\partial r} - \frac{2u}{r^2} \right) \\ & - \lambda_1 \left[ \begin{array}{l} u^2 \frac{\partial^2 u}{\partial r^2} + w^2 \frac{\partial^2 u}{\partial z^2} + 2uw \frac{\partial^2 u}{\partial r \partial z} \\ - \frac{2uw}{r} \frac{\partial v}{\partial r} - \frac{2vw}{r} \frac{\partial v}{\partial z} + \frac{uv^2}{r^2} + \frac{v^2}{r} \frac{\partial u}{\partial r} \end{array} \right] - \frac{\sigma B_0^2}{\rho} \left( u + w \lambda_1 \frac{\partial u}{\partial z} \right), \end{aligned} \quad (3.11)$$

$$\begin{aligned} u \frac{\partial v}{\partial r} + w \frac{\partial v}{\partial z} + \frac{uv}{r} = & \nu \left( \frac{\partial^2 v}{\partial r^2} - \frac{v}{r^2} + \frac{1}{r} \frac{\partial v}{\partial r} + \frac{\partial^2 v}{\partial z^2} \right) \\ & - \lambda_1 \left[ \begin{array}{l} u^2 \frac{\partial^2 v}{\partial r^2} + w^2 \frac{\partial^2 v}{\partial z^2} + 2uw \frac{\partial^2 v}{\partial r \partial z} + \frac{2uw}{r} \frac{\partial u}{\partial r} \\ + \frac{2vw}{r} \frac{\partial u}{\partial z} - \frac{2u^2 v}{r^2} - \frac{v^3}{r^2} + \frac{v^2}{r} \frac{\partial v}{\partial r} \end{array} \right] - \frac{\sigma B_0^2}{\rho} \left( v + w \lambda_1 \frac{\partial v}{\partial z} \right), \end{aligned} \quad (3.12)$$

$$\begin{aligned}
u \frac{\partial w}{\partial r} + w \frac{\partial w}{\partial z} &= -\frac{1}{\rho} \frac{\partial p}{\partial z} - \lambda_1 \left( u^2 \frac{\partial^2 w}{\partial r^2} + 2uw \frac{\partial^2 w}{\partial r \partial z} + w^2 \frac{\partial^2 w}{\partial z^2} + \frac{v^2}{r} \frac{\partial w}{\partial r} \right) \\
&+ \nu \left( \frac{\partial^2 u}{\partial r \partial z} + \frac{\partial^2 w}{\partial r^2} + \frac{1}{r} \frac{\partial u}{\partial z} + \frac{1}{r} \frac{\partial w}{\partial r} + 2 \frac{\partial^2 w}{\partial z^2} \right), \tag{3.13}
\end{aligned}$$

$$u \frac{\partial T}{\partial r} + w \frac{\partial T}{\partial z} = \frac{1}{\rho C_p} \left[ \frac{k(T)}{r} \frac{\partial T}{\partial r} + \frac{\partial}{\partial r} \left( k(T) \frac{\partial T}{\partial r} \right) + \frac{\partial}{\partial z} \left( k(T) \frac{\partial T}{\partial z} \right) \right], \tag{3.14}$$

where  $[u, v, w]$  are the velocity components, kinematic viscosity is depicted by  $\nu$ , the specific heat is  $C_p$ , while the variable thermal conductivity is  $k(T)$ .

$$k(T) = k_\infty \left( 1 + \varepsilon \frac{T - T_2}{T_1 - T_2} \right), \tag{3.15}$$

where  $k_\infty$  is the fluid thermal conductivity and the variable thermal conductivity parameter is  $\varepsilon$ .

The boundary conditions of both lower and upper disks are:

$$\begin{aligned}
u &= s_1 r, \quad v = \Omega_1 r, \quad w = 0, \quad T = T_1, \quad \text{at } z = 0, \\
u &= s_2 r, \quad v = \Omega_2 r, \quad w = 0, \quad T = T_2, \quad \text{at } z = d.
\end{aligned} \tag{3.16}$$

The following transformations are used:

$$\begin{aligned}
u &= \Omega_1 r f'(\eta), \quad v = \Omega_1 r g(\eta), \quad w = -2d\Omega_1 f(\eta), \\
p &= \rho\Omega_1\nu \left( P(\eta) + \frac{1}{2} \frac{r^2}{d^2} \Lambda \right), \quad \theta(\eta) = \frac{T - T_2}{T_1 - T_2}, \quad \eta = \frac{z}{d}.
\end{aligned} \tag{3.17}$$

Using the transformations shown above, Eq. (3.10) is satisfied and the Eqs. (3.11) – (3.14) and (3.16) are written as:

$$f''' - \text{Re} \left( f'^2 - g^2 - 2ff'' \right) + \text{Re} \beta_1 \begin{pmatrix} 4ff'f'' - 4f^2f''' \\ -4fgg' \end{pmatrix} - M \text{Re} (f' - 2\beta_1 f f'') + \Lambda = 0, \tag{3.18}$$

$$g'' + 2 \operatorname{Re} (fg' - f'g) + \operatorname{Re} \beta_1 (4ff'g' - 4f^2g'' + 4ff''g) - M \operatorname{Re} (g - 2\beta_1fg') = 0, \quad (3.19)$$

$$P' + 2f'' + \operatorname{Re} (4ff' - 8\beta_1f^2f'') = 0, \quad (3.20)$$

$$(1 + \varepsilon\theta)\theta'' + 2 \operatorname{Re} \operatorname{Pr} f\theta' + \varepsilon\theta'^2 = 0, \quad (3.21)$$

with the dimensionless boundary constrains:

$$\begin{aligned} f(0) &= 0, & f'(0) &= S_1, & g(0) &= 1, & \theta(0) &= 1, & P(0) &= 1, \\ f(1) &= 0, & f'(1) &= S_2, & g(1) &= \Omega, & \theta(1) &= 0, \end{aligned} \quad (3.22)$$

where  $\Lambda$  is the pressure gradient parameter which is constant. Parameters with no dimensions  $\operatorname{Re}$  shows the Reynolds number,  $\beta_1$  indicates the Deborah number of relaxation time,  $M$  represent the Magnetic parameter, Prandtl number is depicted by  $\operatorname{Pr}$ ,  $S_1$  and  $S_2$  are the stretching parameters of lower and upper disks, and  $\Omega$  indicate the rotational parameter. The mathematical formulas for these non-dimensional values are defined as follows:

$$\begin{aligned} \operatorname{Re} &= \frac{\Omega_1 d^2}{\nu}, & \beta_1 &= \lambda_1 \Omega_1, & M &= \frac{\sigma B_0^2}{\rho \Omega_1}, & \operatorname{Pr} &= \frac{\nu}{\alpha}, \\ S_1 &= \frac{s_1}{\Omega_1}, & S_2 &= \frac{s_2}{\Omega_2}, & \Omega &= \frac{\Omega_2}{\Omega_1}. \end{aligned} \quad (3.23)$$

### 3.2 Nusselt Number

The Nusselt number  $Nu_{r1}$  and  $Nu_{r2}$  values specify the heat transfer rates of rotating disks. Mathematical relations of  $Nu_{r1}$  and  $Nu_{r2}$  are defined as:

$$Nu_{r1} = \frac{dq_w|_{z=0}}{k(T_1 - T_2)}, \quad Nu_{r2} = -\frac{dq_w|_{z=d}}{k(T_1 - T_2)}, \quad (3.24)$$

where

$$q_w = -k \left( \frac{\partial T}{\partial z} \right).$$

In dimensionless form, we can write

$$Nu_{r1} = -\theta'(0), \quad Nu_{r2} = -\theta'(1). \quad (3.25)$$

**Table 3.1** Comparison of  $-\theta'(0)$  for varying values of  $\Omega$  for varying values of  $Re$  and  $\Omega$  when  $S_1 = 0.5, S_2 = 0.0$  and  $M = \beta_1 = 0$ .

| $Re$ | $\Omega$ | $-\theta'(0)$ |           |
|------|----------|---------------|-----------|
| -    | -        | Ref.[67]      | Present   |
| 0    | -0.5     | 1.0508162     | 1.0000000 |
| 10   | -        | 1.0500126     | 1.0500120 |
| 0    | 0.0      | 1.0508162     | 1.0000000 |
| 10   | -        | 1.0558274     | 1.0558270 |
| 0    | 0.5      | 1.0508162     | 1.0000000 |
| 10   | -        | 1.0525851     | 1.0525810 |



**Table 3.2** Nusselt number  $Nu_{r1}$  at the lower disk when  $S_1 = 0.5$ ,  $\beta_1 = 0.1$ ,  $\Omega = 0.5$ .

| $S_2$ | $M$ | $Re$ | $Pr$ | $\epsilon$ | $Nu_{r1}$ |
|-------|-----|------|------|------------|-----------|
| 0.0   | 0.5 | 5.0  | 1.0  | 0.2        | 2.89937   |
| 0.5   | -   | -    | -    | -          | 2.51818   |
| 1.0   | -   | -    | -    | -          | 2.13306   |
| 0.5   | 0.0 | -    | -    | -          | 1.38289   |
| -     | 0.3 | -    | -    | -          | 1.21509   |
| -     | 0.6 | -    | -    | -          | 1.10517   |
| -     | 0.5 | 0.0  | -    | -          | 0.55486   |
| -     | -   | 2.0  | -    | -          | 0.77777   |
| -     | -   | 5.0  | -    | -          | 0.92481   |
| -     | -   | 5.0  | 0.7  | -          | 1.97251   |
| -     | -   | -    | 10   | -          | 1.94481   |
| -     | -   | -    | 20   | -          | 1.92571   |
| -     | -   | -    | 10   | 0.0        | 1.92481   |
| -     | -   | -    | -    | 0.2        | 1.64503   |
| -     | -   | -    | -    | 0.4        | 1.32551   |

**Table 3.3** Validation of  $f''(0)$ ,  $-g'(0)$  and  $\Lambda$  for different estimates of  $\Omega$  in non-stretching cases  $S_1 = S_2 = 0$  when  $Re = 1$  and  $M = \beta_1 = 0$ .

| -         | $\Omega$ | -1.0      | -0.3      | -0.8      | 0.50      | 0.0       |
|-----------|----------|-----------|-----------|-----------|-----------|-----------|
| $f''(0)$  | Ref.[66] | 0.0666600 | 0.1039500 | 0.0839400 | 0.2992378 | 0.0999700 |
| -         | Ref.[67] | 0.0666631 | 0.1039508 | 0.0839420 | 0.0666341 | 0.0999722 |
| -         | Present  | 0.0666625 | 0.1039500 | 0.0839416 | 0.0666340 | 0.0999714 |
| $-g'(0)$  | Ref.[66] | 2.0009500 | 1.3044200 | 1.8025900 | 0.5026100 | 1.0042800 |
| -         | Ref.[67] | 2.0009521 | 1.3044235 | 1.8025884 | 0.5026135 | 1.0042775 |
| -         | Present  | 2.0009520 | 1.3044230 | 1.8025880 | 0.5026135 | 1.0042770 |
| $\Lambda$ | Ref.[66] | 0.1999200 | 0.2063600 | 0.1718500 | 0.5745800 | 0.2992400 |
| -         | Ref.[67] | 0.1999153 | 0.2063572 | 0.1718464 | 0.5745734 | 0.2992364 |
| -         | Present  | 0.1999165 | 0.2063572 | 0.1718472 | 0.5745737 | 0.2992378 |

### 3.3 Numerical Solution

For the numerical computations, the non-dimensional nonlinear momentum, pressure, and temperature Eqs. (3.18) – (3.21) with condition (3.22) are used. Furthermore, the `bvp4c` numerical approach is used to characterise the flow, pressure, and temperature profiles via graphs. In order to estimate the solution of Eqs. (3.18) – (3.121), we must make first assumptions that fulfill the boundary condition (3.22). The ordinary differential equations is transformed by introducing specific new variables to use this numerical built-in method. The conversion steps are as follows:

$$\begin{aligned}
 f &= y_1, & f' &= y_2, & f'' &= y_3, & f''' &= yy_1, & g &= y_4, & g' &= y_5, & g'' &= yy_2, \\
 P &= y_6, & P' &= yy_3, & \theta &= y_7, & \theta' &= y_8, & \theta'' &= yy_4.
 \end{aligned}$$

$$yy_1 = \frac{\text{Re} [(y_2^2 - y_4 - 2y_1y_3) - \beta_1 (4y_1y_2y_3 - 4y_1y_4y_5) + M(y_2 - 2\beta_1y_1y_3)] - \Lambda}{(1 - 4 \text{Re} \beta_1 y_1^2)}, \quad (3.26)$$

$$yy_2 = \frac{\text{Re} [2 (y_4 y_2 - y_1 y_5) - \beta_1 (4y_1 y_2 y_5 + 4y_1 y_3 y_4) + M (y_4 - 2\beta_1 y_1 y_5)]}{(1 - 4 \text{Re} \beta_1 y_1^2)}, \quad (3.27)$$

$$yy_3 = \text{Re} (-4y_1 y_2 + 8\beta_1 y_1^2 y_3) - 2y_3, \quad (3.28)$$

$$yy_4 = \frac{-2 \text{Re} \text{Pr} y_1 y_8 - \varepsilon y_8^2}{(1 + \varepsilon y_7)}, \quad (3.29)$$

with boundary conditions

$$\begin{aligned} y_1(0) &= 0, & y_2(0) &= S_1, & y_4(0) &= 1, & y_6(0) &= 1, & y_7(0) &= 1 \\ y_1(1) &= 0, & y_2(1) &= S_2, & y_4(1) &= \Omega, & y_7(1) &= 0. \end{aligned} \quad (3.30)$$

### 3.4 Discussion

This section shows numerical results for radial  $f'(\eta)$ , azimuthal  $g(\eta)$ , and axial  $f(\eta)$  velocities, pressure  $P(\eta)$ , and temperature  $\theta(\eta)$  profiles for different rotation parameters  $\Omega$ , stretching parameters  $(S_1, S_2)$ , Deborah number  $\beta_1$ , Reynolds number  $\text{Re}$ , Magnetic field number  $M$ , Prandtl number  $\text{Pr}$ , and heat transfer parameter  $\varepsilon$ . Further, all graphs are drawn for rotation parameter  $\Omega = -0.5$  (solid lines) and  $\Omega = 0.5$  (dashed lines) respectively.

Tables 3.1 and 3.3 represent the comparison of  $f''(0)$ ,  $g'(0)$ ,  $\theta'(0)$ , and  $\Lambda$ . For the validation of results with pervious publications, Tables 3.1 and 3.3 are added.

Table 3.2 illustrated the rate of heat transfer  $Nu_{r1}$  at the lower disk for the parameters  $S_2$ ,  $M$ ,  $\text{Re}$ ,  $\text{Pr}$ ,  $\varepsilon$ . As the values of Prandtl number  $\text{Pr}$ , and Reynold number  $\text{Re}$  rasies the nusselt number enhance. While the stretching parameter  $S_2$ , magnetic parameter  $M$ , and thermal conductivity parameter  $\varepsilon$  increases effects to decreases in heat transfer rate.

Figs 3.2(a) – 3.2(d) are drawn to depict the influence of upper disk stretching parameter  $S_2$  on axial  $f(\eta)$ , radial  $f'(\eta)$ , and azimuthal  $g(\eta)$  velocities along with temperature profile  $\theta(\eta)$  while taking the lower disk stretching parameter  $S_1$  constant ( $S_1 = 0$ ). It is reveal from Figs 3.2(a) and 3.2(b) the axial and radial velocity profile reduces for higher values of  $S_2$ . However, Figs 3.2(c) – 3.2(d) depicts that both the azimuthal velocity and temperature profile enhances for increasing  $S_2$ .

Figs 3.3(a) – 3.3(d) are portrayed to visualize the velocities and temperature profile for

stretching parameter  $S_2$  by taking  $S_1 = 0.5$ . Figs 3.2(a) and 3.2(b) reveal that the axial and radial velocity profiles decreasing for increasing values of  $S_2$ . The magnitude of axial velocity upsuges, the upper disk pushes more fluid axially, but a greater quantity of radial fluid is thrown out rapidly to spinning disk. Figs 3.3(c)–3.3(d) demonstrate the behaviour of azimuthal velocity and temperature profile. When the stretching ratios of coaxially disks increses, the azimuthal velocity and temperature profile shows increasing trend.

The impact of magnetic parameter  $M$  on the flow velocities and fluid temperature depicted on the Figs 3.4(a) – 3.4(d). Both the disks stretched in the same direction ( $S_1, S_2 = 0.5$ ). In Figs 3.4(a) – 3.4(c) represents the decreasing trend on axial, radial and azimuthal velocities with stronger magnetic field. When the magnetic field produces a resistive force that slows fluid velocity, the fluid temperature rises, that are shown in Fig 3.4(d). Physically, increasing magnetic parameter tends to ehance the Lorentz force and the strong Lorentz force generates grater friction to the transport phenomenon.

Figs 3.5(a) – 3.5(c) illustrate the impact of Reynold number  $Re$  on fluid velocities and temperature profile with the assumption that both the disks are stretched at the same time ( $S_1, S_2 = 0.5$ ). The examine the influence of the Reynolds number on the components of radial and azimuthal velocity is seen in Figs 3.5(a) and 3.5 (b) . When the Reynold number rises, then both the velocities shows an increasing trend. The fluid temperature in Fig 3.5(c) dwindled for escalating estimates Reynolds number  $Re$  due to a reduction in viscosity.

The upshorts of Deborah number  $\beta_1$  on flow and temperature fields when the both disks rotates in the same direction ( $\Omega = 0.5$ ) with the stretching rate  $S_2 = 0$ , are shown in Figs 3.6(a) – 3.6(d). The flow behaviour in the axial  $f(\eta)$ , radial  $f'(\eta)$  and azimuthal  $g(\eta)$  is represented in decreasing order in Figs 3.6(a) – 3.6(c). Fluids tends to behave as a viscoelastic solid material with an increasing Deborah number. The fluid temperature  $\theta(\eta)$  increases slightly within the disks, as seen in Fig 3.6(d).

In Figs 3.7(a) and 3.7(b) demonstrate that the behaviour of temperature field for the thermal conductivity parameter  $\varepsilon$  and the Prandtl number  $Pr$ . Higher values of  $\varepsilon$  causes the fluid temperature to rise, as illustrated in Fig 3.7(a). Mounting of the fluid thermal conductivity for larger values of  $\varepsilon$ . Hence, higher heat is generated and transfered from the disk surface to the fluid, increasing the temperature profile. The dashed-dotted lines in Fig 3.7(b) depict the

temperature profile for  $(S_1 = 0.5, S_2 = 0)$ . As the Prandtl number  $Pr$  increases the temperature profile decreases. The solid lines for  $(S_1 = S_2 = 0.5)$  show that the temperature field decreases. The dashed lines for  $(S_1 = 0.0, S_2 = 0.5)$  demonstrate that the temperature curves rises as  $Pr$  rises.

Figs 3.8(a) – 3.8(b) depicts the pressure field  $P(\eta)$  for the various values of magnetic parameter  $M$  and stretching rate parameter  $S_2$ . Fig. 3.8(a) the pressure field  $P(\eta)$  is observed to diminish in order with mounting estimates of magnetic parameter  $M$ . In Fig. 3.8(b) the pressure field rises with the stretching ratio  $S_2$  increases, after a certain height in the direction of the upper disk the pressure field declines.

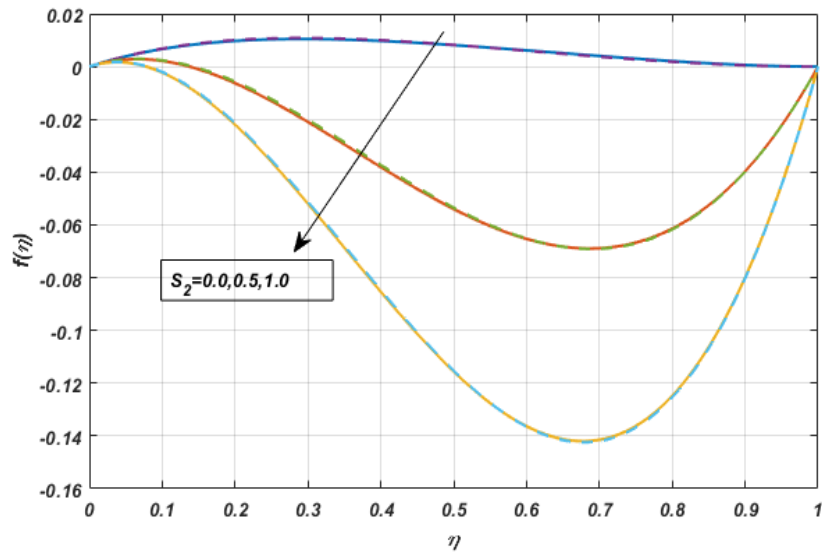


Fig. 3.2(a)  $f(\eta)$  against  $S_2$ ,

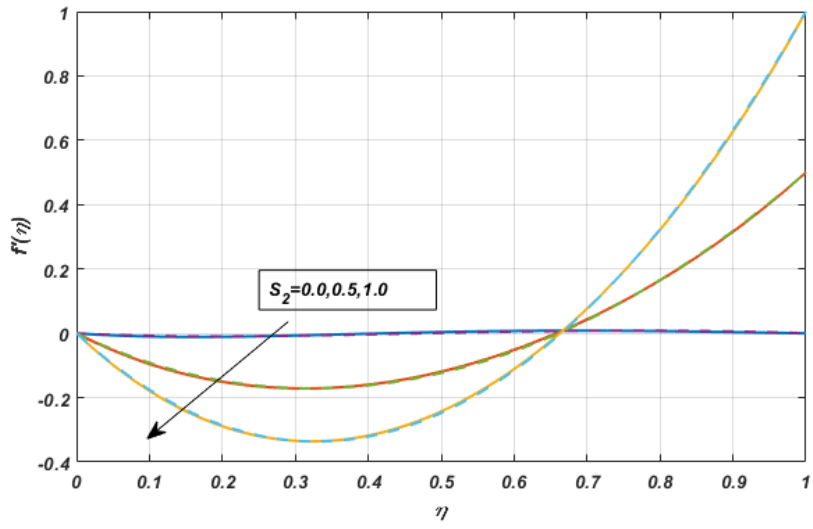


Fig. 3.2(b)  $f'(\eta)$  against  $S_2$ ,

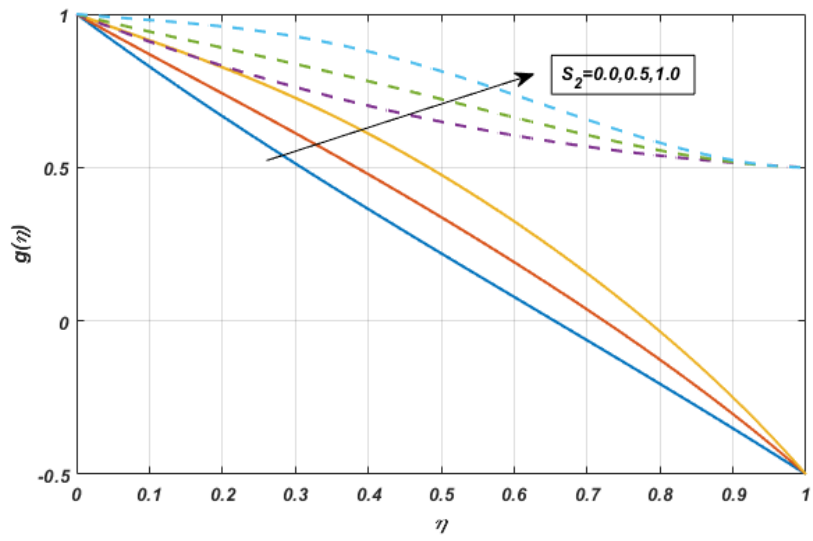


Fig. 3.2(c)  $g(\eta)$  against  $S_2$ ,

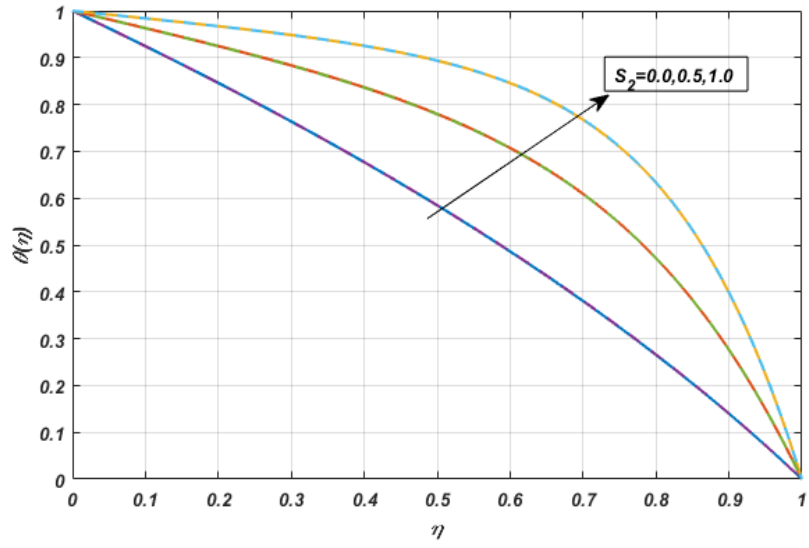


Fig 3.2(d)  $\theta(\eta)$  against  $S_2$ ,

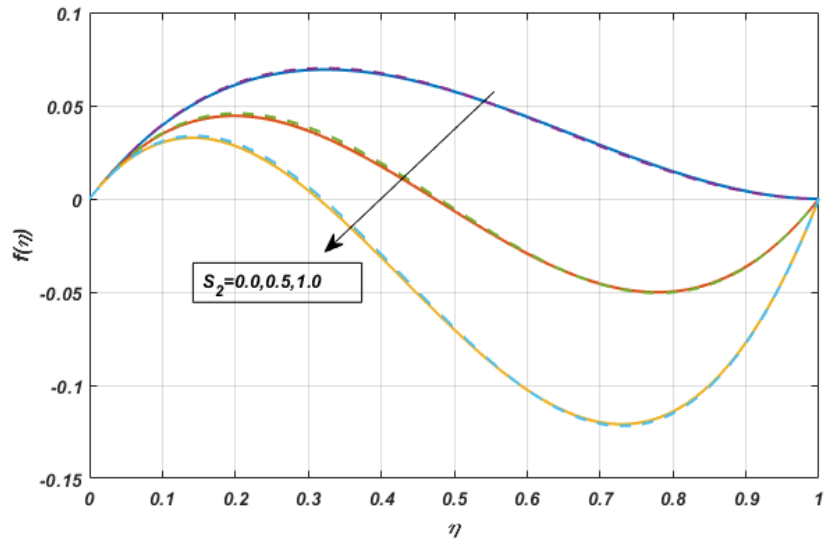


Fig. 3.3(a)  $f(\eta)$  against  $S_2$ ,

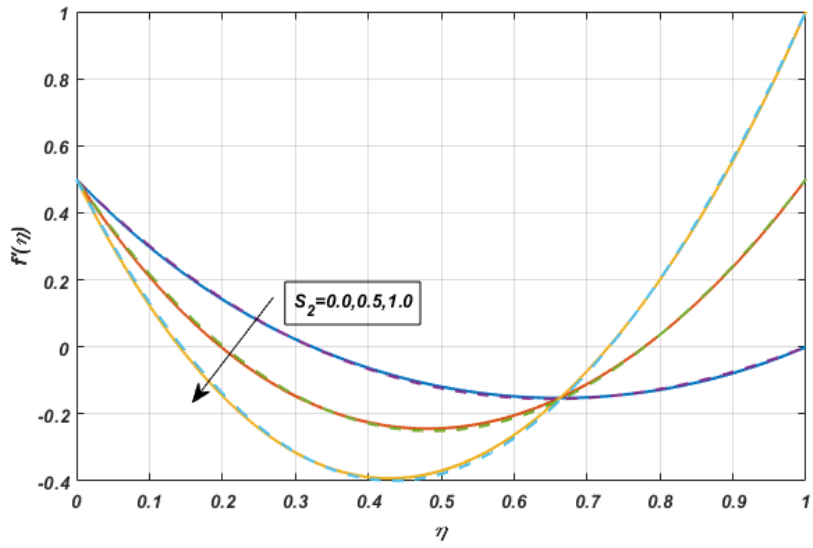


Fig. 3.3(b)  $f'(\eta)$  against  $S_2$ ,

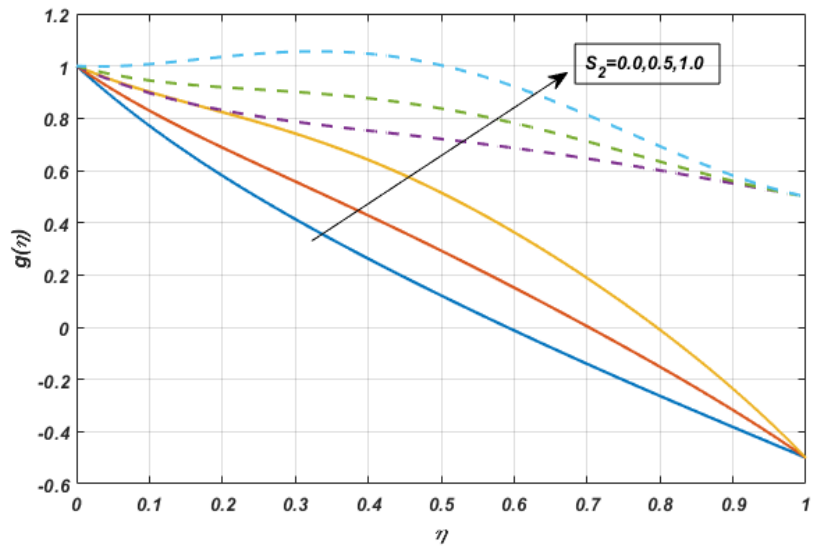


Fig. 3.3(c)  $g(\eta)$  against  $S_2$ ,



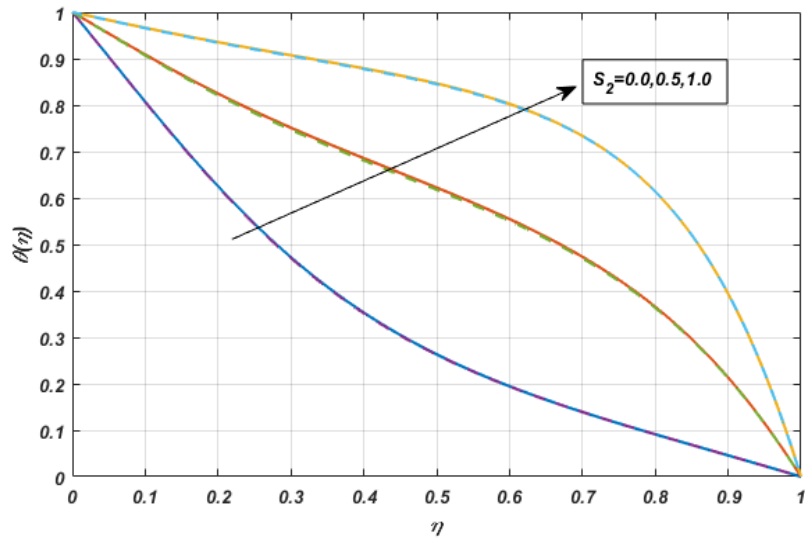


Fig. 3.3(d)  $\theta(\eta)$  against  $S_2$ ,

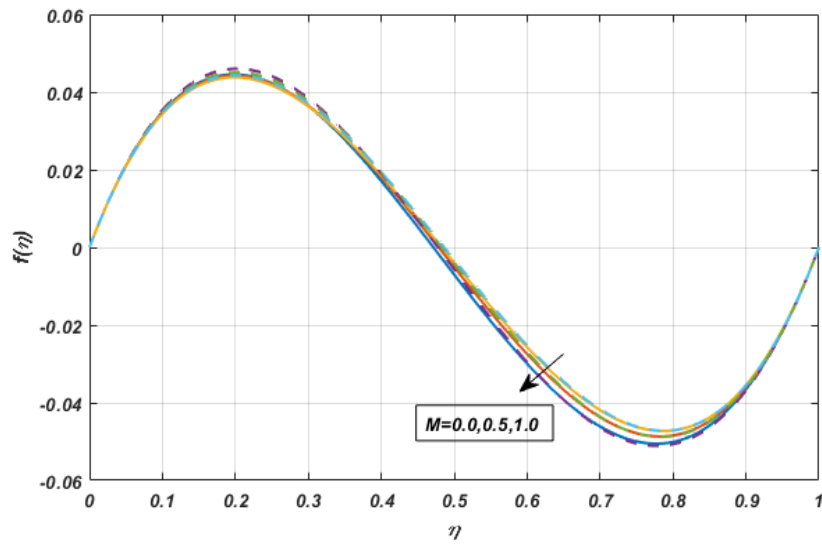


Fig. 3.4(a)  $f(\eta)$  against  $M$ ,

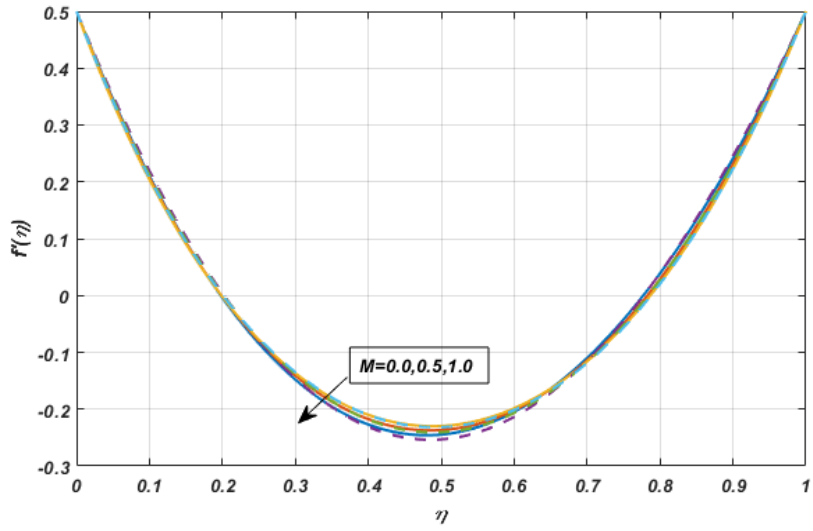


Fig. 3.4(b)  $f'(\eta)$  against  $M$ ,

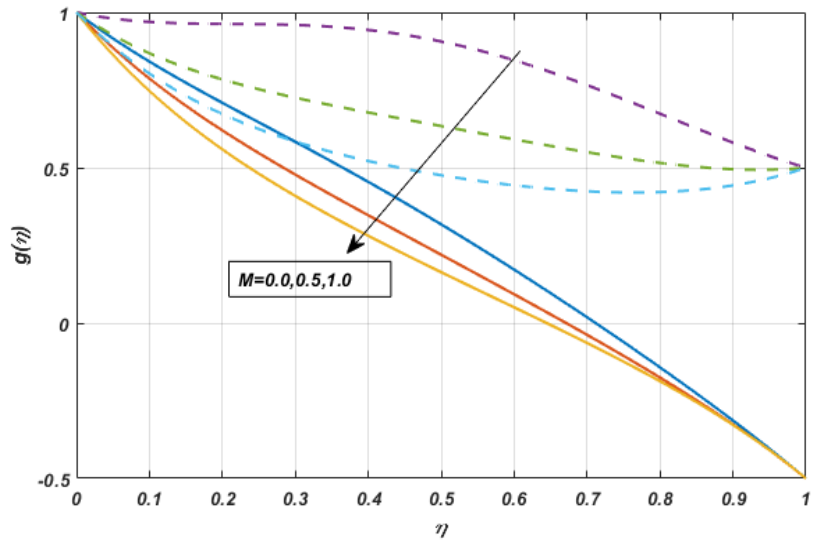


Fig. 3.4(c)  $g(\eta)$  against  $M$ ,

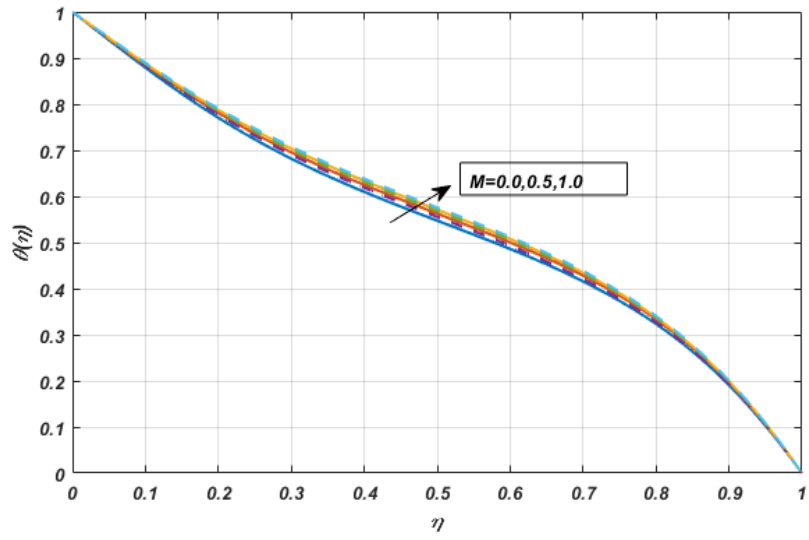


Fig. 3.4(d)  $\theta(\eta)$  against  $M$ ,

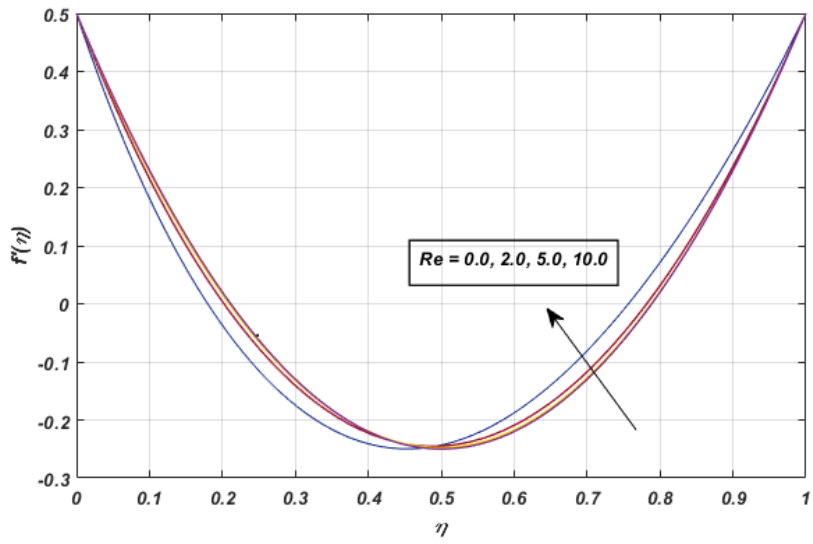


Fig. 3.5(a)  $f'(\eta)$  against  $Re$ ,

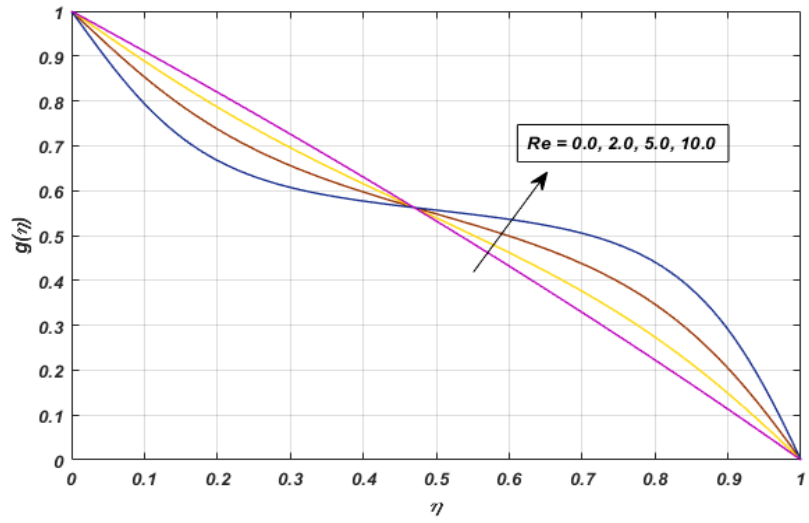


Fig. 3.5(b)  $g(\eta)$  against  $Re$ ,

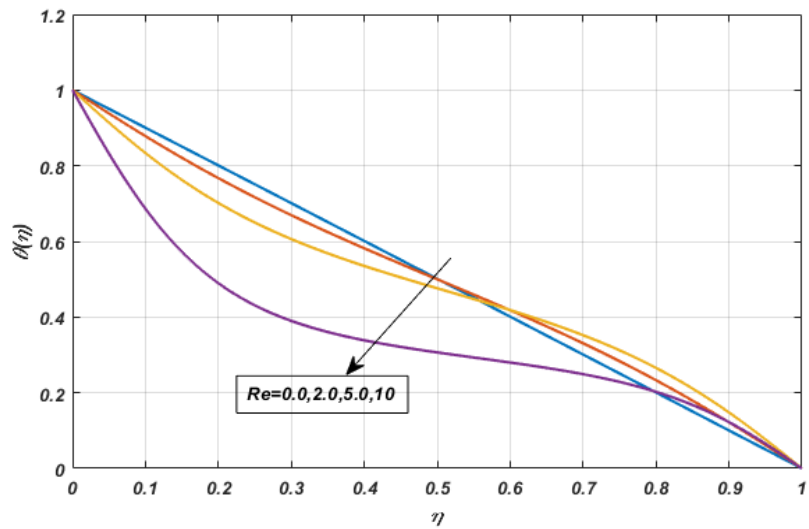


Fig. 3.5(c)  $\theta(\eta)$  against  $Re$ ,

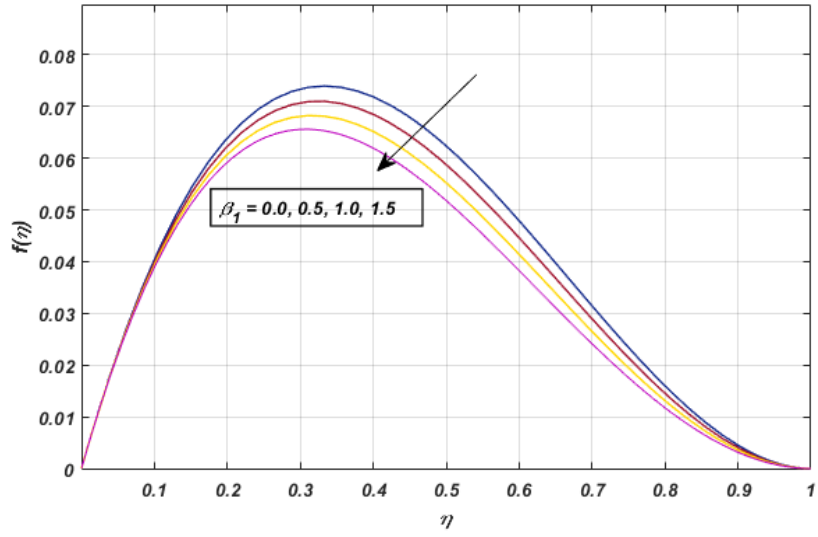


Fig. 3.6(a)  $f(\eta)$  against  $\beta_1$ ,

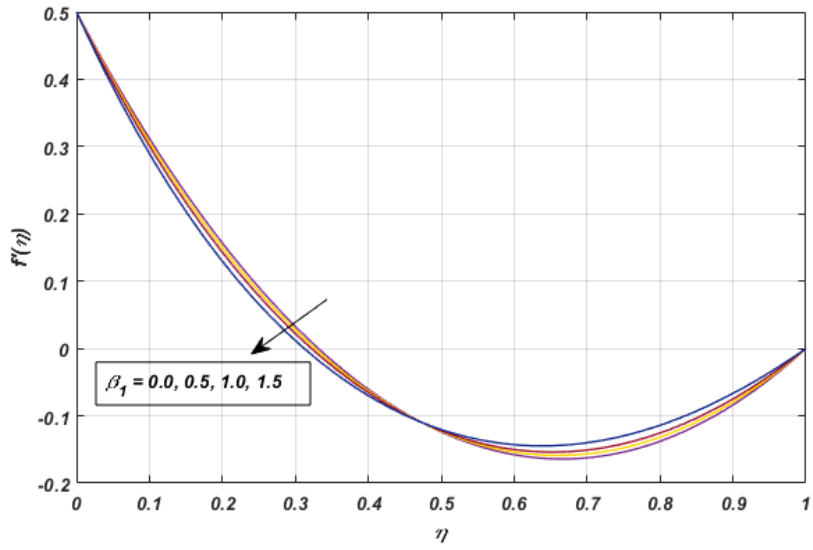


Fig. 3.6(b)  $f'(\eta)$  against  $\beta_1$ ,

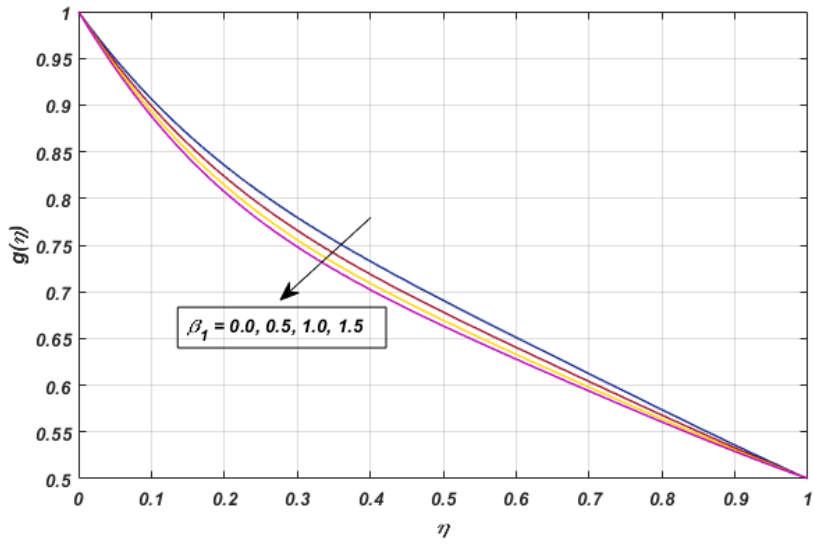


Fig. 3.6(c)  $g(\eta)$  against  $\beta_1$ ,

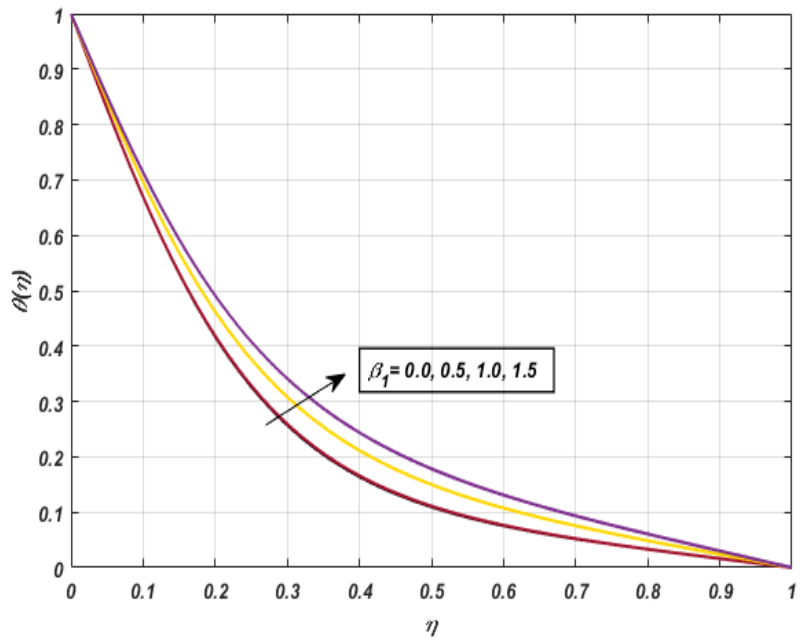


Fig. 3.6(d)  $\theta(\eta)$  against  $\beta_1$ ,

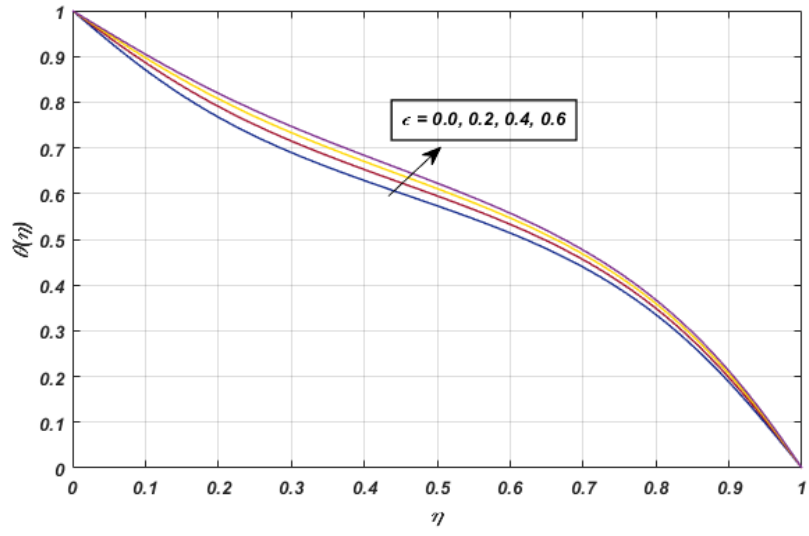


Fig. 3.7(a)  $\theta(\eta)$  against  $\epsilon$ ,

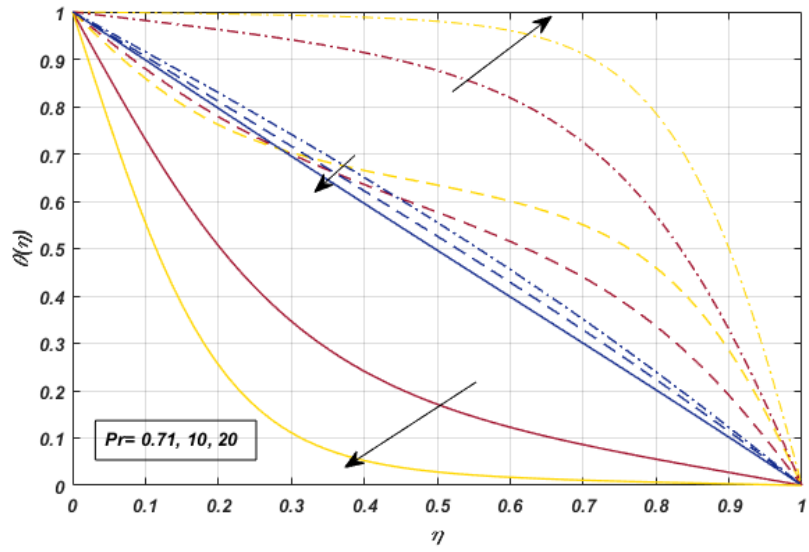


Fig. 3.7(b)  $\theta(\eta)$  against  $Pr$ ,

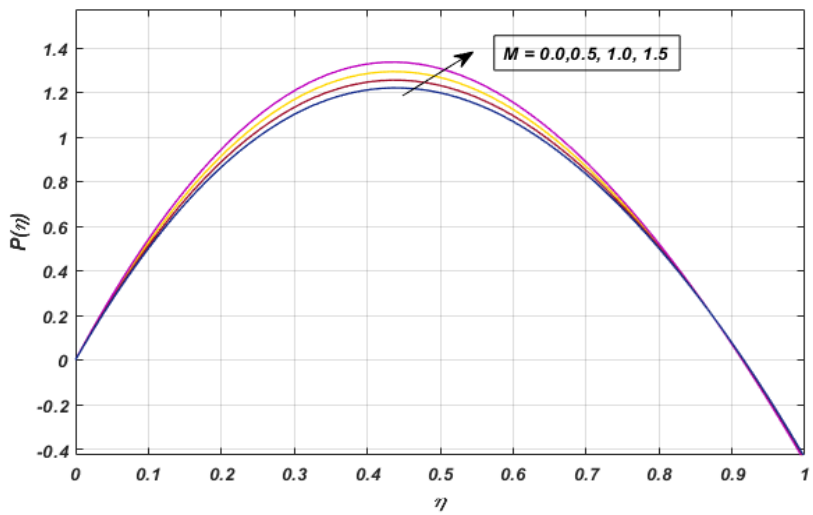


Fig. 3.8(a)  $P(\eta)$  against  $M$ ,

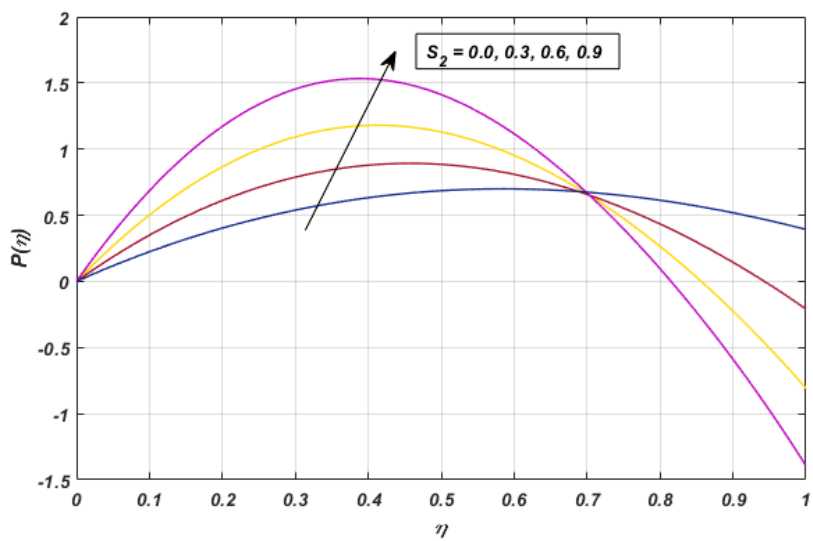


Fig. 3.8(b)  $P(\eta)$  against  $S_2$ ,



## Chapter 4

# **HALL CURRENT AND ION SLIP IMPACT ON A OLDROYD-B NANOFLUID FLOW DRIVEN BY TWO CONCENTRIC ROTATING DISKS WITH CATTANEO-CHRISTOV HEAT FLUX**

This study examines the effects of an axisymmetric spinning disks on an Oldroyd-B nanofluid flow. Relaxation and retardation times characteristics are the unique feature of the present viscoelastic type fluid model. The Buongiorno model is used to investigate bioconvection in two stretched spinning disks. Magnetohydrodynamics is applied parallel to the normal surface. MHD effect is so strong that the Hall current and ion-slip effects can't be ignored. The addition of gyrotactic microorganisms in the nanofluid increases the stability of

the nanoparticles. To deal with nondimensional problem equations, similarity transformations are applied. The governing equations are numerically computed by using bvp4c technique in MATLAB software. Graphical representations are used to highlight the importance of flow parameters in the pattern of velocity, temperature, concentration, and gyrotactic microorganism. At both surfaces of disks, the numerical simulations for Nusselt, Sherwood numbers, and motile microorganism are also carried out.

## 4.1 Mathematical modelling

We consider an Oldroyd-B fluid flow that is stable, incompressible, and three-dimensional. The fluid flow is considered between two disks, both disks are stretching and spinning. The lower disk is at  $z = 0$ , whereas the upper disk is at  $z = d$ .  $C_1$  and  $C_2$  are the concentrations and  $T_1$  and  $T_2$  are the temperatures of lower and upper disks respectively. Both disks are rotating in anticlockwise direction with angular velocities  $\Omega_1$  (lower) and  $\Omega_2$  (upper). The stretching rates for the lower and upper disks are denoted by  $s_1$  and  $s_2$ , respectively (see Fig 4.1). Magnetic field is applied along the  $z$ -axis. The heat and mass transmission phenomenon are observed using convective boundary conditions. The effects of gyrotactic microorganisms is also observed. The flow of geometry is shown in Fig 4.1. The flow is governed by the laws of conservation of mass, momentum, energy, concentration, and gyrotactic microorganism which are described as:

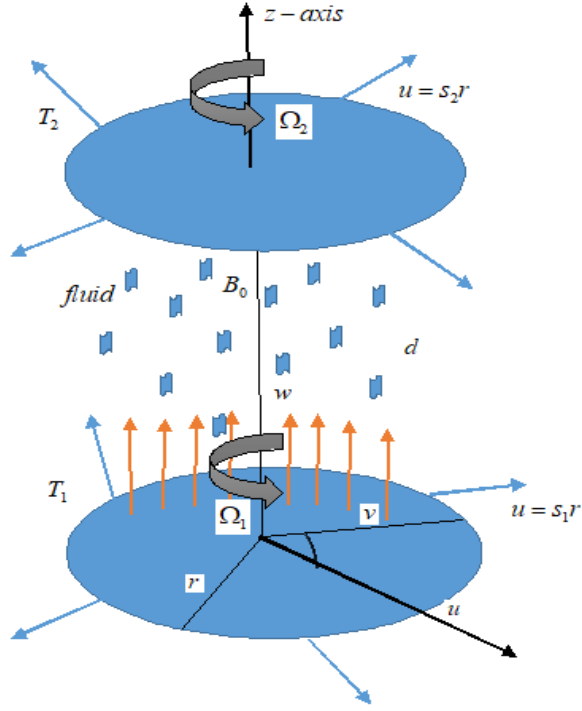


Fig 4.1 Geometry of the flow

The Oldroyd-B fluid model stress tensor is expressed as:

$$\left(1 + \lambda_1 \frac{D}{Dt}\right) \mathbf{S} = \mu \left(1 + \lambda_2 \frac{D}{Dt}\right) \mathbf{A}_1, \quad (4.1)$$

where  $\mathbf{S}$  denotes the extra stress tensor,  $\mu$  is the dynamic viscosity,  $\lambda_1$  shows the relaxation and  $\lambda_2$  the retardation times. The mathematical relationships for conservation of mass and momentum in an incompressible MHD fluid flow are:

$$\nabla \cdot \mathbf{V} = 0, \quad (4.2)$$

$$\rho \mathbf{a} = -\nabla p + \nabla \cdot \mathbf{S} + \mathbf{J} \times \mathbf{B}, \quad (4.3)$$

where the material time derivative is denoted  $\mathbf{a}$  for the vector  $\mathbf{V}$  velocity.

$$\mathbf{a} = \frac{d\mathbf{V}}{dt} = \frac{\partial\mathbf{V}}{\partial t} + (\mathbf{V} \cdot \nabla) \mathbf{V}, \quad (4.4)$$

where the density of the fluid is denoted by  $\rho$  and  $p$  is the pressure, with the equation (4.1) diverging on both sides.

$$\left(1 + \lambda_1 \frac{D}{Dt}\right) \nabla \cdot \mathbf{S} = \mu \left(1 + \lambda_2 \frac{D}{Dt}\right) \nabla \cdot \mathbf{A}_1, \quad (4.5)$$

after applying the operator  $\left(1 + \lambda_1 \frac{D}{Dt}\right)$  on equation (4.3) and using the result of equation (4.5), we have

$$\rho \left(1 + \lambda_1 \frac{D}{Dt}\right) \mathbf{a} = - \left(1 + \lambda_1 \frac{D}{Dt}\right) \nabla p + \mu \left(1 + \lambda_2 \frac{D}{Dt}\right) \nabla \cdot \mathbf{A}_1 + \left(1 + \lambda_1 \frac{D}{Dt}\right) (\mathbf{J} \times \mathbf{B}), \quad (4.6)$$

where  $\mathbf{A}_1 = \nabla \mathbf{V} + (\nabla \mathbf{V})^t$  is the first Rivlin-Ericksen tensor and  $\frac{D}{Dt}$  the upper convective derivative. Using the cylindrical polar coordinates system  $(r, \varphi, z)$  for mathematical modelling. The velocity vector for axisymmetric steady flow is:

$$\mathbf{V} = [u(r, z), v(r, z), w(r, z)]. \quad (4.7)$$

where  $u, v,$  and  $w$  are radial, azimuthal, and axial velocity components, respectively. The system of differential equations are:

$$\frac{\partial u}{\partial r} + \frac{\partial w}{\partial z} + \frac{u}{r} = 0, \quad (4.8)$$

$$\begin{aligned}
u \frac{\partial u}{\partial r} + w \frac{\partial u}{\partial z} - \frac{v^2}{r} &= -\frac{1}{\rho} \frac{\partial p}{\partial r} + \nu \left( 2 \frac{\partial^2 u}{\partial r^2} + \frac{\partial^2 u}{\partial z^2} + \frac{2}{r} \frac{\partial u}{\partial r} + \frac{\partial^2 w}{\partial r \partial z} - \frac{2u}{r^2} \right) \\
&\quad - \frac{\sigma \beta_0^2}{\rho (\alpha^2 + \beta_h^2)} \left( 1 + w \lambda_1 \frac{\partial u}{\partial z} \right) (\alpha u - \beta_h v) \\
&\quad - \lambda_1 \left[ \begin{aligned} &u^2 \frac{\partial^2 u}{\partial r^2} + w^2 \frac{\partial^2 u}{\partial z^2} + 2uw \frac{\partial^2 u}{\partial r \partial z} - \\ &\frac{2uv}{r} \frac{\partial v}{\partial r} - \frac{2vw}{r} \frac{\partial v}{\partial z} + \frac{uv^2}{r^2} + \frac{v^2}{r} \frac{\partial u}{\partial r} \end{aligned} \right] \\
&\quad + \nu \lambda_2 \left[ \begin{aligned} &4 \frac{u^2}{r^3} - 2 \frac{w}{r^2} \frac{\partial u}{\partial z} - \frac{1}{r} \left( \frac{\partial u}{\partial z} \right)^2 - 2 \frac{\partial u}{\partial z} \frac{\partial^2 w}{\partial z^2} + w \frac{\partial^3 u}{\partial z^3} \\ &- 2 \frac{u}{r^2} \frac{\partial u}{\partial r} - \frac{\partial u}{\partial r} \frac{\partial^2 u}{\partial z^2} - \frac{2}{r} \left( \frac{\partial u}{\partial r} \right)^2 - \frac{1}{r} \frac{\partial u}{\partial z} \frac{\partial w}{\partial r} + 2 \frac{w}{r} \frac{\partial^2 u}{\partial r \partial z} \\ &- \frac{\partial u}{\partial r} \frac{\partial^2 u}{\partial r \partial z} + u \frac{\partial^3 u}{\partial r \partial z^2} + w \frac{\partial^3 w}{\partial r \partial z^2} + 2 \frac{u}{r} \frac{\partial^2 u}{\partial r^2} - 2 \frac{\partial u}{\partial r} \frac{\partial^2 u}{\partial r^2} \\ &+ u \frac{\partial^3 w}{\partial r^2 \partial z} + 2w \frac{\partial^3 u}{\partial r^2 \partial z} + 2u \frac{\partial^3 u}{\partial r^3} - \frac{\partial u}{\partial z} \frac{\partial^2 w}{\partial r^2} - \frac{\partial u}{\partial r} \frac{\partial^2 w}{\partial r \partial z} \end{aligned} \right], \quad (4.9)
\end{aligned}$$

$$\begin{aligned}
u \frac{\partial v}{\partial r} + w \frac{\partial v}{\partial z} + \frac{uv}{r} &= \nu \left( \frac{\partial^2 v}{\partial r^2} + \frac{1}{r} \frac{\partial v}{\partial r} - \frac{v}{r^2} + \frac{\partial^2 v}{\partial z^2} \right) - \frac{\sigma \beta_0^2}{\rho (\alpha^2 + \beta_h^2)} \left( 1 + w \lambda_1 \frac{\partial v}{\partial z} \right) (\alpha v + \beta_h u) \\
&\quad - \lambda_1 \left[ \begin{aligned} &u^2 \frac{\partial^2 v}{\partial r^2} + w^2 \frac{\partial^2 v}{\partial z^2} + 2uw \frac{\partial^2 v}{\partial r \partial z} + 2 \frac{uv}{r} \frac{\partial u}{\partial r} \\ &+ 2 \frac{vw}{r} \frac{\partial u}{\partial z} - 2 \frac{u^2 v}{r^2} - \frac{v^3}{r^2} + \frac{v^2}{r} \frac{\partial v}{\partial r} \end{aligned} \right] \\
&\quad + \nu \lambda_2 \left[ \begin{aligned} &u \frac{\partial^3 v}{\partial r^3} + u \frac{\partial^3 v}{\partial r \partial z^2} + 2 \frac{v}{r} \frac{\partial^2 u}{\partial r^2} + \frac{v}{r} \frac{\partial^2 u}{\partial z^2} \\ &+ \frac{v}{r} \frac{\partial^2 w}{\partial r \partial z} + 2 \frac{v}{r^2} \frac{\partial u}{\partial r} + w \frac{\partial^3 v}{\partial r^2 \partial z} - \frac{w}{r^2} \frac{\partial v}{\partial z} + \frac{w}{r} \frac{\partial^2 v}{\partial r \partial z} \\ &+ w \frac{\partial^3 v}{\partial z^3} - \frac{\partial v}{\partial r} \frac{\partial^2 w}{\partial r \partial z} - \frac{2}{r} \frac{\partial u}{\partial r} \frac{\partial v}{\partial r} + \frac{uv}{r^3} - \frac{u}{r^2} \frac{\partial v}{\partial r} \\ &- 2 \frac{\partial v}{\partial r} \frac{\partial^2 u}{\partial r^2} - \frac{\partial v}{\partial r} \frac{\partial^2 u}{\partial z^2} - \frac{u}{r} \frac{\partial^2 v}{\partial z^2} - \frac{\partial v}{\partial z} \frac{\partial^2 u}{\partial r \partial z} \\ &- \frac{\partial v}{\partial z} \frac{\partial^2 w}{\partial r^2} - \frac{1}{r} \frac{\partial u}{\partial z} \frac{\partial v}{\partial z} - \frac{1}{r} \frac{\partial v}{\partial z} \frac{\partial w}{\partial r} - 2 \frac{\partial v}{\partial z} \frac{\partial^2 w}{\partial z^2} \end{aligned} \right], \quad (4.10)
\end{aligned}$$

$$\begin{aligned}
u \frac{\partial w}{\partial r} + w \frac{\partial w}{\partial z} &= -\frac{1}{\rho} \frac{\partial p}{\partial z} + \nu \left( \frac{\partial^2 w}{\partial r^2} + \frac{\partial^2 u}{\partial r \partial z} + \frac{1}{r} \frac{\partial w}{\partial r} + \frac{1}{r} \frac{\partial u}{\partial z} + 2 \frac{\partial^2 w}{\partial z^2} \right) \\
&\quad - \lambda_1 \left( u^2 \frac{\partial^2 w}{\partial r^2} + w^2 \frac{\partial^2 w}{\partial z^2} + 2uw \frac{\partial^2 w}{\partial r \partial z} + \frac{v^2}{r} \frac{\partial w}{\partial r} \right) \\
&\quad + \nu \lambda_2 \left[ \begin{aligned}
&u \frac{\partial^3 u}{\partial r^2 \partial z} + u \frac{\partial^3 w}{\partial r^3} - \frac{u}{r^2} \frac{\partial u}{\partial z} + \frac{u}{r} \frac{\partial^2 u}{\partial r \partial z} + \frac{u}{r^2} \frac{\partial w}{\partial r} - 2 \frac{\partial w}{\partial z} \frac{\partial^2 w}{\partial z^2} \\
&\quad + \frac{u}{r} \frac{\partial^2 w}{\partial r^2} + 2u \frac{\partial^3 w}{\partial r \partial z^2} + w \frac{\partial^3 u}{\partial r \partial z^2} + w \frac{\partial^3 w}{\partial r^2 \partial z} + \frac{w}{r} \frac{\partial^2 u}{\partial z^2} \\
&\quad + \frac{w}{r} \frac{\partial^2 w}{\partial r \partial z} + 2w \frac{\partial^3 w}{\partial z^3} - 2 \frac{\partial w}{\partial r} \frac{\partial^2 u}{\partial r^2} - \frac{\partial w}{\partial r} \frac{\partial^2 u}{\partial z^2} - \frac{\partial w}{\partial r} \frac{\partial^2 w}{\partial r \partial z} \\
&\quad - \frac{2}{r} \frac{\partial w}{\partial r} \frac{\partial u}{\partial r} - \frac{\partial w}{\partial z} \frac{\partial^2 u}{\partial r \partial z} - \frac{\partial w}{\partial z} \frac{\partial^2 w}{\partial r^2} - \frac{1}{r} \frac{\partial w}{\partial z} \frac{\partial w}{\partial r} - \frac{1}{r} \frac{\partial w}{\partial z} \frac{\partial u}{\partial r}
\end{aligned} \right], \quad (4.11)
\end{aligned}$$

$$\begin{aligned}
u \frac{\partial T}{\partial r} + w \frac{\partial T}{\partial z} &= \alpha^* \left( \frac{\partial^2 T}{\partial r^2} + \frac{1}{r} \frac{\partial T}{\partial r} + \frac{\partial^2 T}{\partial z^2} \right) + \tau \left[ \begin{aligned}
&D_B \left( \frac{\partial T}{\partial r} \frac{\partial C}{\partial r} + \frac{\partial T}{\partial z} \frac{\partial C}{\partial z} \right) \\
&\quad + \frac{D_T}{T_2} \left\{ \left( \frac{\partial T}{\partial r} \right)^2 + \left( \frac{\partial T}{\partial z} \right)^2 \right\}
\end{aligned} \right] \\
&\quad - \gamma \left[ \begin{aligned}
&u^2 \frac{\partial^2 T}{\partial r^2} + w^2 \frac{\partial^2 T}{\partial z^2} + 2uw \frac{\partial^2 T}{\partial z \partial r} + \left( u \frac{\partial u}{\partial r} + w \frac{\partial u}{\partial z} \right) \frac{\partial T}{\partial r} \\
&\quad + \left( u \frac{\partial w}{\partial r} + w \frac{\partial w}{\partial z} \right) \frac{\partial T}{\partial z}
\end{aligned} \right], \quad (4.12)
\end{aligned}$$

$$u \frac{\partial C}{\partial r} + w \frac{\partial C}{\partial z} - D_B \left( \frac{\partial^2 C}{\partial r^2} + \frac{1}{r} \frac{\partial C}{\partial r} + \frac{\partial^2 C}{\partial z^2} \right) = \frac{D_T}{T_2} \left( \frac{1}{r} \frac{\partial T}{\partial r} + \frac{\partial^2 T}{\partial r^2} + \frac{\partial^2 T}{\partial z^2} \right), \quad (4.13)$$

$$u \frac{\partial N}{\partial r} + w \frac{\partial N}{\partial z} + \frac{bw_c}{C_1 - C_2} \left( \frac{\partial N}{\partial z} \frac{\partial C}{\partial z} + N \frac{\partial^2 C}{\partial z^2} \right) = D_n \left( \frac{\partial^2 N}{\partial r^2} + \frac{1}{r} \frac{\partial N}{\partial r} + \frac{\partial^2 N}{\partial z^2} \right). \quad (4.14)$$

With suitable boundary conditions

$$\begin{aligned}
u &= s_1 r, \quad \frac{\partial u}{\partial z} = 0, \quad v = \Omega_1 r, \quad w = 0, \quad k_f \frac{\partial T}{\partial z} = -h_1 (T_1 - T), \\
N &= N_1, \quad C = C_1, \quad \text{at } z = 0, \\
u &= s_2 r, \quad \frac{\partial u}{\partial z} = 0, \quad v = \Omega_2 r, \quad w = 0, \quad k_f \frac{\partial T}{\partial z} = -h_2 (T - T_2), \\
N &= N_2, \quad C = C_2, \quad \text{at } z = d,
\end{aligned} \quad (4.15)$$

where  $(u, v, w)$  are the velocities taken along  $(r, \varphi, z)$  direction respectively.  $p$  is the pressure,  $\sigma$  is the electrical conductivity,  $T$  shows the temperature and  $C$  is the concentration of the fluid, the Brownian diffusion coefficient is denoted by  $D_B$ ,  $D_T$  denotes the thermophoretic diffusion coefficient,  $\nu$  shows the kinematic viscosity,  $\alpha^*$  represents the thermal diffusivity,  $\alpha = 1 + \beta_i \beta_h$ , where  $\beta_i$  and  $\beta_h$  denotes the ion-slip and Hall current parameter respectively. Dimensionless form of above mathematical model is obtained by utilizing following transformations:

$$\begin{aligned} \eta &= \frac{z}{d}, \quad \theta(\eta) = \frac{T - T_2}{T_1 - T_2}, \quad \phi(\eta) = \frac{C - C_2}{C_1 - C_2}, \quad h(\eta) = \frac{N - N_2}{N_1 - N_2}, \\ u &= r\Omega_1 f'(\eta), \quad v = r\Omega_1 g(\eta), \quad w = -2d\Omega_1 f(\eta), \quad p = \rho\Omega_1 \nu \left( P(\eta) + \frac{1}{2} \frac{r^2}{d^2} \Lambda \right). \end{aligned} \quad (4.16)$$

using the above transformation, the Eq. (4.8) is satisfied and the dimensionless form of Eqs. (4.9) – (4.14)

$$\begin{aligned} &f''' - 4 \operatorname{Re} \beta_1 f (f f''' - f' f'' + g g') + 2\beta_2 (f''^2 - f f^{iv}) - \operatorname{Re} (f'^2 - 2f f'' - g^2) \\ &- \frac{\operatorname{Re} M}{\alpha^2 + \beta_h^2} \begin{pmatrix} \alpha (f' - 2\beta_1 f f'') \\ -\beta_h (g - 2f g' \beta_1) \end{pmatrix} - \Lambda = 0, \end{aligned} \quad (4.17)$$

$$\begin{aligned} &g'' - 4 \operatorname{Re} \beta_1 (f^2 g'' - f f' g' - f f'' g) + \beta_2 (2f'' g - 2f g''') - \operatorname{Re} (2f' g + 2f g') \\ &- \frac{\operatorname{Re} M}{\alpha^2 + \beta_h^2} \begin{pmatrix} \alpha (g - 2\beta_1 f g') \\ -\beta_h (f' - 2\beta_1 f f'') \end{pmatrix} = 0, \end{aligned} \quad (4.18)$$

$$P' + 4f'' - 8 \operatorname{Re} \beta_1 f^2 f'' - \beta_2 (4f f''' - 4f f'') - 4 \operatorname{Re} f f' = 0, \quad (4.19)$$

$$\theta'' + 2 \operatorname{Re} \operatorname{Pr} f \theta' + \operatorname{Pr} N_b \theta' \phi' + \operatorname{Pr} N_t \theta'^2 - 4 \operatorname{Re} \operatorname{Pr} \lambda (f^2 \theta'' + f f' \theta') = 0, \quad (4.20)$$

$$\phi'' + \frac{N_t}{N_b} \theta'' + 2Le \operatorname{Re} \operatorname{Pr} f \phi' = 0, \quad (4.21)$$

$$h'' + 2 \operatorname{Re} Sc f h' - Pe (h' \phi' + (h + \Omega^*) \phi'') = 0. \quad (4.22)$$

With transformed boundary conditions

$$\begin{aligned} f(0) &= 0, \quad f''(0) = 0, \quad g(0) = 1, \quad f'(0) = S_1, \quad \theta'(0) = -\beta_{i1}(1 - \theta), \\ \phi(0) &= 1, \quad h(0) = 1, \quad P(0) = 0, \quad \text{at } z = 0, \\ f''(1) &= 0, \quad f'(1) = S_2, \quad g(1) = \Omega, \quad \theta'(1) = -\beta_{i2}\theta, \\ \phi(1) &= 0, \quad h(1) = 0 \quad \text{at } z = d. \end{aligned} \quad (4.23)$$

where  $\Lambda$  is the unknown pressure gradient parameter.  $\operatorname{Re}, \beta_1, \beta_2, M, \operatorname{Pr}, N_t, N_b, Le, Sc, Pe$  represents Reynold number, Deborah number of relaxation and retardation time parameters, Magnetic parameter, the Prandtl number, Thermophoresis parameter, Brownian motion parameter, Lewis parameter, Schmidt number, and Peclet number respectively.  $S_1, S_2$  are the stretching parameters.  $\Omega$  is the rotation parameter.  $\beta_{i1}, \beta_{i2}$  are the thermal Biot numbers.  $\Omega^*$  is the motile microorganism difference parameter.

$$\begin{aligned} \operatorname{Re} &= \frac{\Omega_1 d^2}{\nu}, \quad M = \frac{\sigma \beta_0^2}{\rho \Omega_1}, \quad \operatorname{Pr} = \frac{\nu}{\alpha^*}, \quad N_t = \frac{\tau D_T (T_1 - T_2)}{k T_2}, \quad N_b = \frac{\tau D_B (C_1 - C_2)}{k}, \\ Pe &= \frac{b w_c}{D_n}, \quad Sc = \frac{\nu}{D_B}, \quad \lambda = \Omega_1 \gamma, \quad \beta_1 = \lambda_1 \Omega_1, \quad \beta_2 = \lambda_2 \Omega_1, \quad S_1 = \frac{s_1}{\Omega_1}, \\ S_2 &= \frac{s_2}{\Omega_1}, \quad \Omega = \frac{\Omega_1}{\Omega_2}, \quad \Omega^* = \frac{N_2}{N_1 - N_2}, \quad Le = \frac{\alpha^*}{D_B}, \quad \beta_{i1} = \frac{h_1 d}{k_f}, \quad \beta_{i2} = \frac{h_2 d}{k_f}. \end{aligned} \quad (4.24)$$

## 4.2 Important physical quantities

The significant of emerging quantities such as Nusselt numbers, Sherwood numbers, and motile microorganism flux.  $Nu_{r1}$  and  $Nu_{r2}$  specify the rate of heat transfer at the lower and upper disks, respectively.  $Sh_{r1}$  and  $Sh_{r2}$  shows the rate of mass transfer of both disks.  $Nn_{r1}$  and  $Nn_{r2}$  specify the density of microorganism.  $Nu_{r1}, Nu_{r2}, Sh_{r1}, Sh_{r2}, Nn_{r1}$  and  $Nn_{r2}$  are mathematical relations in dimensional form are defined by:



$$\begin{aligned}
Nu_{r1} &= \frac{dq_w|_{z=0}}{k(T_1 - T_2)}, & Nu_{r2} &= \frac{dq_w|_{z=d}}{k(T_1 - T_2)}, \\
Sh_{r1} &= \frac{dq_m|_{z=0}}{D_B(C_1 - C_2)}, & Sh_{r2} &= \frac{dq_m|_{z=d}}{D_B(C_1 - C_2)}, \\
Nn_{r1} &= \frac{dq_n|_{z=0}}{D_n(N_1 - N_2)}, & Nn_{r2} &= \frac{dq_n|_{z=d}}{D_n(N_1 - N_2)}.
\end{aligned} \tag{4.25}$$

where

$$\begin{aligned}
q_w &= -k \left( \frac{\partial T}{\partial z} \right) = \frac{-k(T_1 - T_2)}{d} \theta' (0), \\
q_m &= -D_B \left( \frac{\partial C}{\partial z} \right) = \frac{-D_B(C_1 - C_2)}{d} \phi' (0), \\
q_n &= -D_n \left( \frac{\partial N}{\partial z} \right) = \frac{-D_n(N_1 - N_2)}{d} h' (0).
\end{aligned}$$

In dimensionless form, we can write

$$\begin{aligned}
Nu_{r1} &= -\theta'(0), & Nu_{r2} &= -\theta'(1), \\
Sh_{r1} &= -\phi'(0), & Sh_{r2} &= -\phi'(1), \\
Nn_{r1} &= -h'(0), & Nn_{r2} &= -h'(1).
\end{aligned} \tag{4.26}$$

### 4.3 Numerical approach

Eqs. (4.17)–(4.22) with BCs (4.23) form a nonlinear system of ordinary differential equations (ODEs). We employ a numerical approach called bvp4c Matlab scheme to solve these nonlinear differential equations. The numerical simulation are as follows:

$$\begin{aligned}
f &= y_1, f' = y_2, f'' = y_3, f''' = y_4, f'''' = yy_1, g = y_5, g' = y_6, g'' = y_7, g''' = yy_2, \\
P &= y_8, P' = yy_3, \theta = y_9, \theta' = y_{10}, \theta'' = yy_4, \phi = y_{10}, \phi' = y_{11}, \phi'' = yy_5, \\
h &= y_{12}, h' = y_{13}, h'' = yy_6.
\end{aligned}$$

$$yy_1 = \frac{1}{2\beta_2 y_1} \left[ \begin{array}{c} y_4 - \text{Re } \beta_1 (4y_1^2 y_3 - 4y_1 y_2 y_3 + 4y_1 y_5 y_6) + 2\beta_2 y_3^2 \\ - \text{Re} (y_2^2 - y_5^2 - 2y_1 y_3) - \frac{M \text{Re}}{\alpha^2 + \beta_h^2} \begin{pmatrix} \alpha (y_2 - 2\beta_1 y_1 y_3) \\ -\beta_h (y_5 - 2\beta_1 y_1 y_6) \end{pmatrix} - \Lambda \end{array} \right], \quad (4.27)$$

$$yy_2 = \frac{1}{2\beta_2 y_1} \left[ \begin{array}{c} y_7 - \text{Re } \beta_1 (4y_1^2 y_7 - 4y_1 y_2 y_6 - 4y_1 y_3 y_5) + 2\beta_2 y_3 y_6 \\ - \text{Re} (2y_2 y_5 + 2y_1 y_6) - \frac{M \text{Re}}{\alpha^2 + \beta_h^2} \begin{pmatrix} \alpha (y_5 - 2\beta_1 y_1 y_6) \\ -\beta_h (y_2 - 2\beta_1 y_1 y_3) \end{pmatrix} \end{array} \right], \quad (4.28)$$

$$yy_3 = -4y_3 - 8 \text{Re } \beta_1 y_1^2 y_3 + \beta_2 (4y_1 y_4 - 4y_1 y_3) + 4 \text{Re } y_1 y_2, \quad (4.29)$$

$$yy_4 = \frac{-1}{1 - 4\lambda \text{Re } \text{Pr } y_1^2} (2 \text{Re } \text{Pr } y_1 y_{10} + \text{Pr } N_b y_{10} y_{12} + \text{Pr } N_t y_{10}^2 - 4 \text{Re } \text{Pr } \lambda y_1 y_2 y_{10}), \quad (4.30)$$

$$yy_5 = - \left( \frac{N_t}{N_b} yy_4 + 2 \text{Pr } \text{Re } L e y_1 y_{12} \right), \quad (4.31)$$

$$yy_6 = - (2 \text{Re } S c y_1 y_{14} - P e (y_{12} y_{13} + (y_{13} + \Omega^*) yy_5)). \quad (4.32)$$

## 4.4 Discussion

This section discusses the results of graphical representations of radial, azimuthal velocities, temperature, concentration, and microorganism profile for various parameters. We will also investigate the effect of these characteristics on the rate of heat, mass transfer and motile flux.

Fig 4.2 shows the effect of  $\beta_1$  on  $f'(\eta)$ . It is discovered that the velocity of Oldroyd-B nanofluid  $f'(\eta)$  increases for mounting values of relaxation time parameter  $\beta_1$ . Fig 4.3 depicts the influence of Deborah parameter of retardation time  $\beta_2$  on radial velocity  $f'(\eta)$ . When strain under continuous stress declines, which causes the velocity to decrease on a rising trend of the retardation time parameter  $\beta_2$  (0.2, 0.4, 0.6, 0.8).

Fig 4.4 is drawn to observe the variation in azimuthal velocity  $g(\eta)$  caused by the effect of relaxation time parameter  $\beta_1$ . For increasing values of the relaxation time parameter  $\beta_1$  (0.2, 0.4, 0.6, 0.8), the azimuthal velocity rises while all other parameters remain constant. The Deborah number of relaxation time  $\beta_1$  is the ratio of material relaxation time to the material observation time. As a result, the azimuthal velocity  $g(\eta)$  increases on an increasing trend of

relaxation time parameter  $\beta_1$ . Fig 4.5 depicts the effect of Deborah parameter of retardation time  $\beta_2$  on azimuthal velocity  $g(\eta)$  is presented. With the increment of  $\beta_2$  (0.2, 0.4, 0.6, 0.8), the azimuthal velocity  $g(\eta)$  is decreased.

The consequences of Brownian motion  $N_b$  on the fluid temperature  $\theta(\eta)$  are shown in Fig 4.6. The temperature  $\theta(\eta)$  enhances mounting values of  $N_b$  (0.80, 1.80, 2.80, 3.80). Higher rates of Brownian motion parameter  $N_b$  raise the Brownian diffusion coefficient  $D_B$ . Brownian motion is the primary goal of the current system. Brownian motion is caused by the random motion of nanoparticles, which causes the temperature to rise. The system obtains the parameter Pr by assigning the specified values to improve the temperature displayed in Fig 4.7. Physically, increasing the Prandtl number increases thermal diffusivity. Figs 4.8 and 4.9 depict the effect of thermal Biot numbers  $\beta_{i1}$  and  $\beta_{i2}$  on the temperature profile. The Biot number typically indicates whether or not the temperature within a body will change greatly. By increasing the values of  $\beta_{i1}$  and  $\beta_{i2}$ , the temperature profile varies significantly.

Lewis number  $Le$  is one of the active properties of nanofluids.  $Le$  play a significant impact in mass transfer characteristics. Fig 4.10 illustrates that  $\phi(\eta)$  decreases as the Lewis number  $Le$  increases, ensuring the power of nanoparticle diffusion. Lewis number  $Le$  is negatively related to nanoparticle diffusion. In Fig 4.11 shows the thermophoresis parameter  $N_t$  that reduces the nanoparticle concentration  $\phi(\eta)$ . By applying the temperature, thermophoresis pushes the nanoparticles from a high energy state to a low energy state, which effects the concentration.

Heating impacts the system and increases the formation of bioconvection. To demonstrate the influence of Peclet number  $Pe$  over the motile density, Fig 4.12 sketched are portrait. It is observed that for the larger values of  $Pe$ , the motile density increases. Fluid motile density increases at higher  $Pe$  due to an increment in the diffusivity of microorganisms. Fig 4.13 displays the concentration of motile microorganisms  $h(\eta)$  on the Schmidt number  $Sc$ . Increasing  $Sc$  values decrease the concentration profile  $h(\eta)$ . Fig 4.14 shows that when the Lewis number  $Le$  increases, the concentration of motile microorganisms  $h(\eta)$  increases. It is related to a rise in the density and thickness of the boundary layer of motile microorganisms.

In Table 4.1 shows the values of Nusselt number  $-\theta'(0)$ , the Sherwood number  $-\phi'(0)$  and motile microorganism  $-h'(0)$  are calculated numerically against different parameters of  $N_t$ ,  $N_b$ ,  $\beta_1$ , and  $\beta_2$ . Observations shows that  $-\theta'(0)$  decreases for increasing  $N_t$  and  $\beta_1$ , while

increasing trend obtained by increasing in  $N_b$  and  $\beta_2$ . The mass transfer rate  $-\phi'(0)$  declines against  $N_b$  and  $\beta_2$ , respectively while an opposite trends are noticed against  $N_t$  and  $\beta_1$ . The motile microorganism  $-h'(0)$  decreaseses for  $N_t, N_b, \beta_1, \beta_2$ .

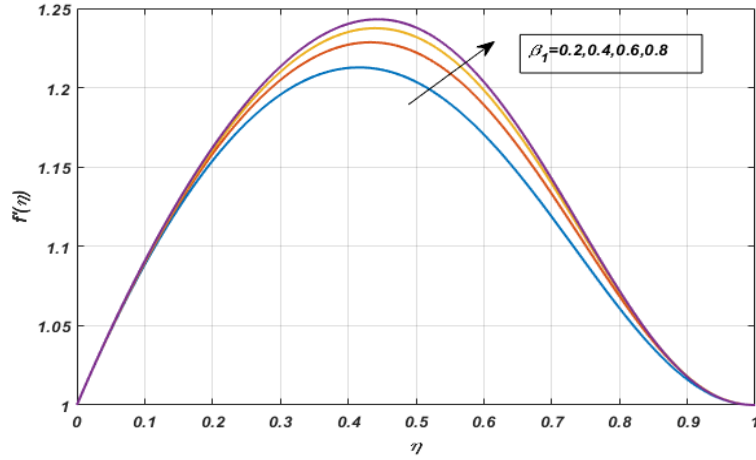


Fig. 4.2  $f'(\eta)$  against  $\beta_1$ ,

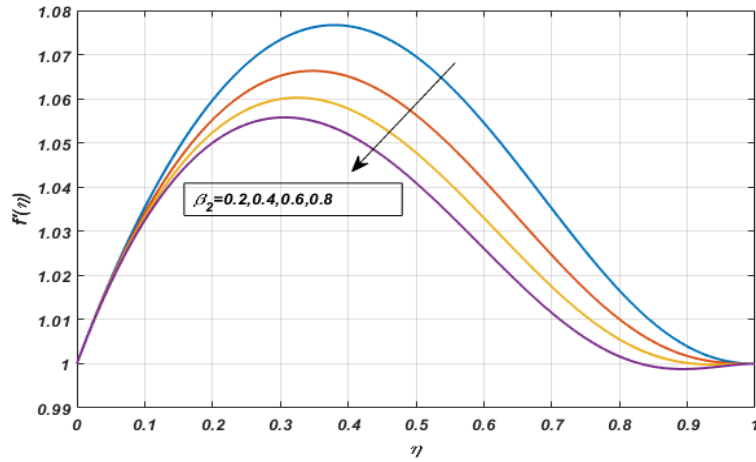


Fig. 4.3  $f'(\eta)$  against  $\beta_2$ ,

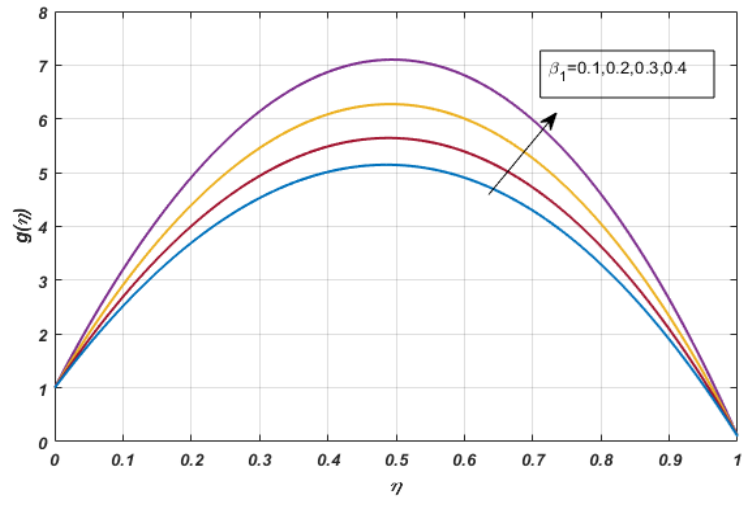


Fig. 4.3  $g(\eta)$  against  $\beta_1$ ,

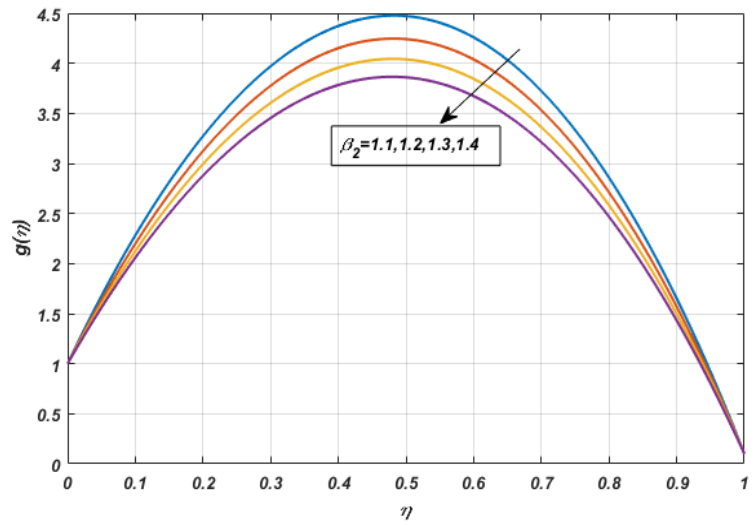


Fig. 4.4  $g(\eta)$  against  $\beta_2$ ,

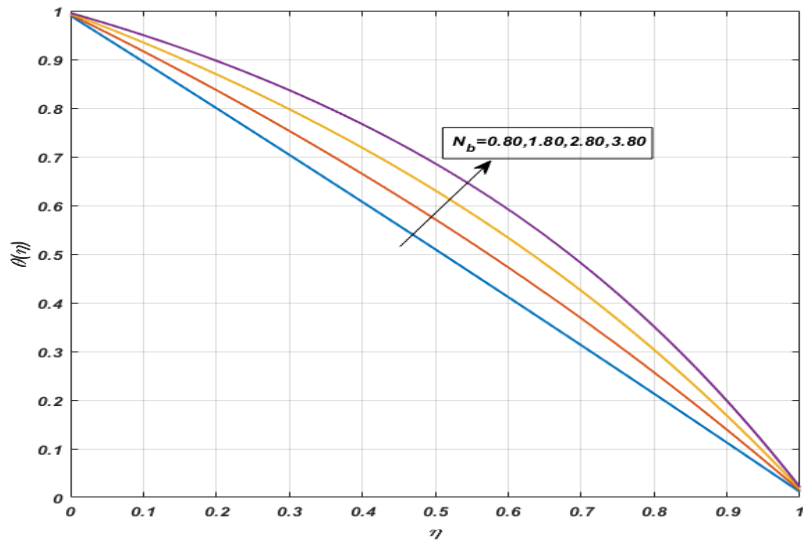


Fig. 4.6  $\theta(\eta)$  against  $N_b$ ,

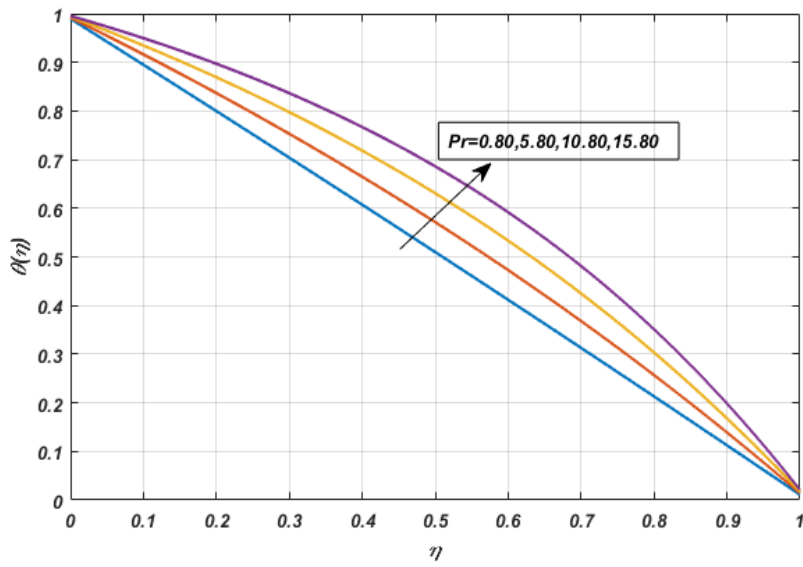


Fig. 4.7  $\theta(\eta)$  against  $Pr$ ,

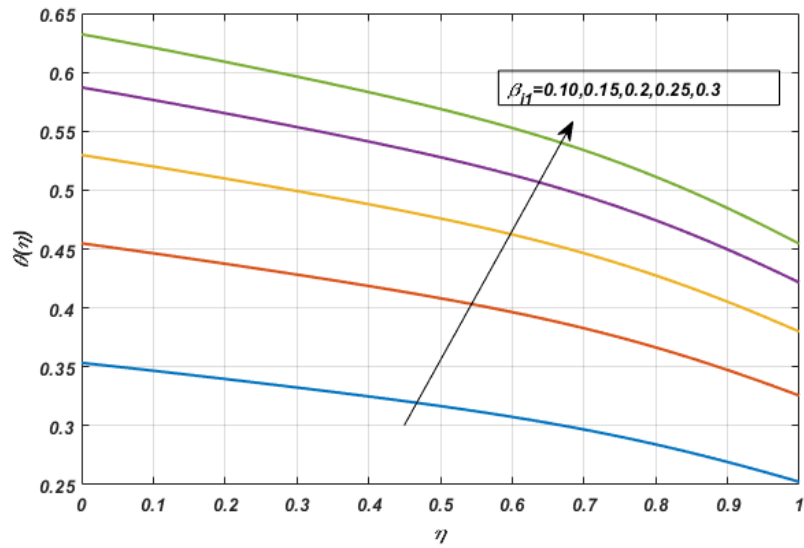


Fig. 4.8  $\theta(\eta)$  against  $\beta_{i1}$ ,

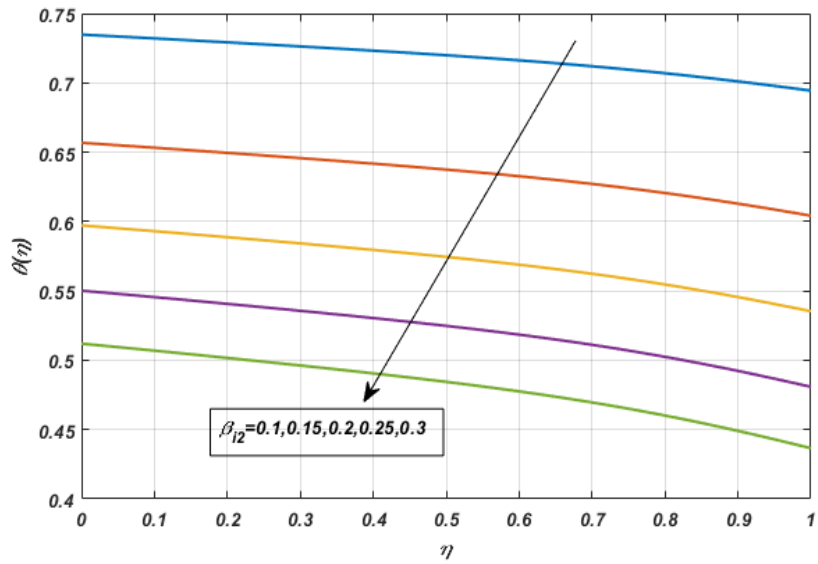


Fig. 4.9  $\theta(\eta)$  against  $\beta_{i2}$ ,

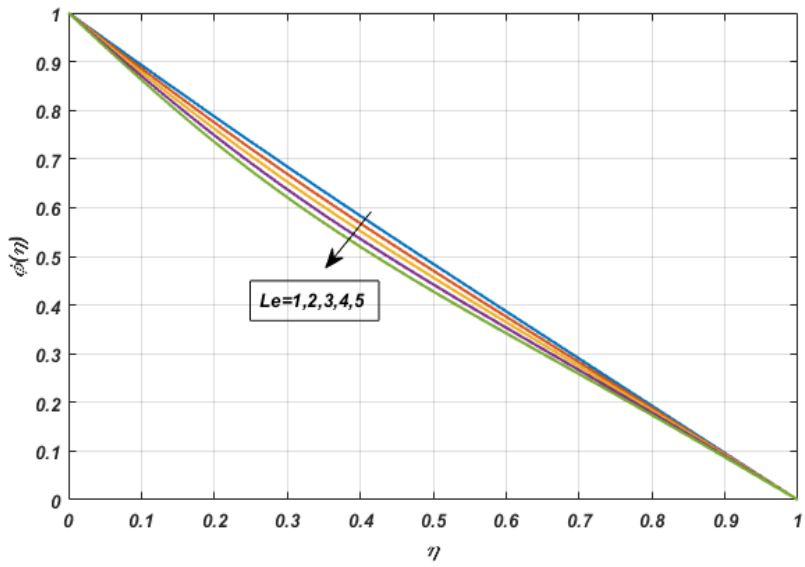


Fig. 4.10  $\phi(\eta)$  against  $Le$ ,

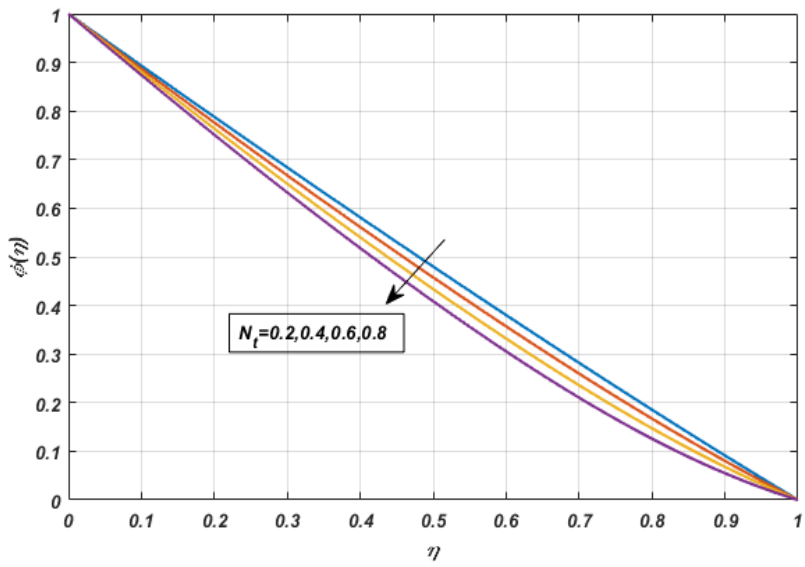


Fig. 4.11  $\phi(\eta)$  against  $N_t$ ,



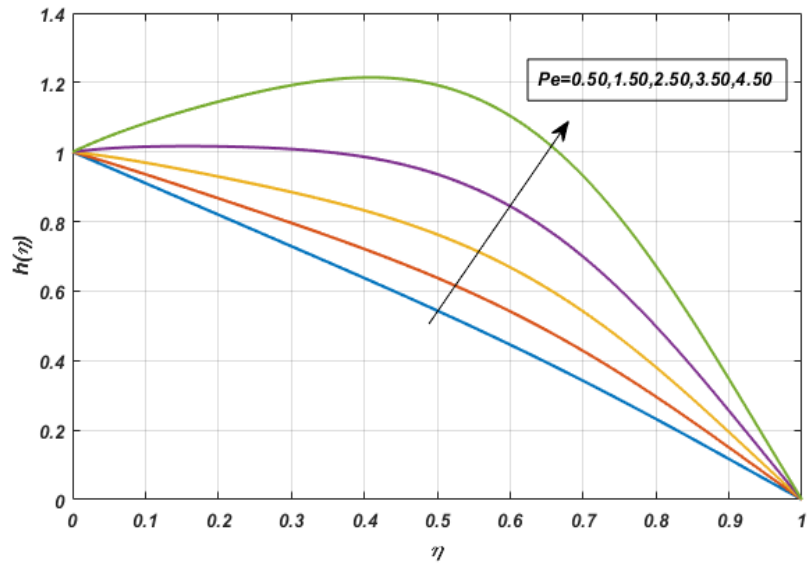


Fig. 4.12  $h(\eta)$  against  $Pe$ ,

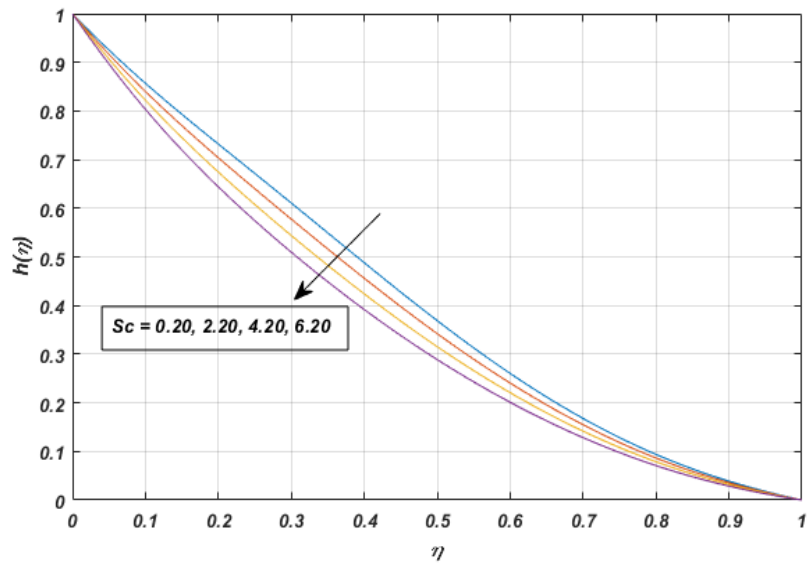


Fig. 4.13  $h(\eta)$  against  $Sc$ ,

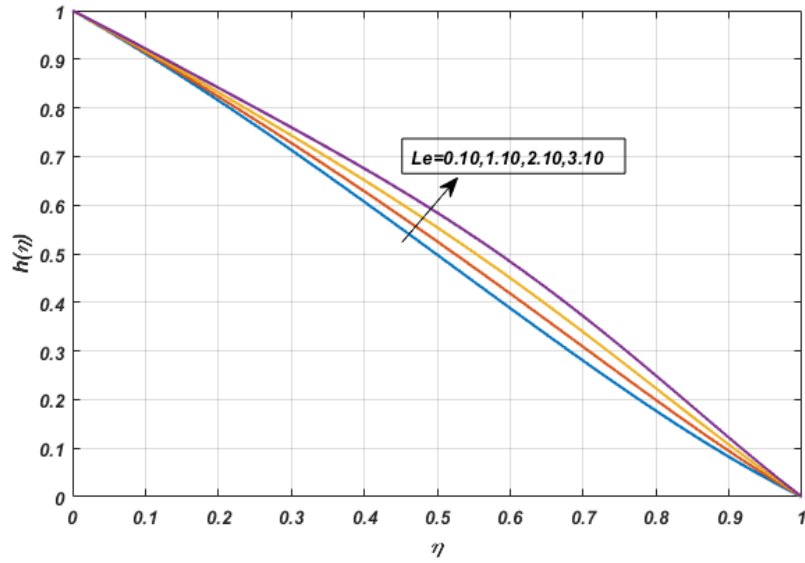


Fig. 4.14  $h(\eta)$  against  $Le$ .

**Table 4.1.** Numerical values of  $-\theta'(0)$ ,  $-\phi'(0)$ , and  $-h'(0)$ .

| $N_t$ | $N_b$ | $\beta_1$ | $\beta_2$ | $-\theta'(0)$ | $-\phi'(0)$ | $-h'(0)$ |
|-------|-------|-----------|-----------|---------------|-------------|----------|
| 0.1   | 0.1   | 0.03      | 0.03      | 0.482720      | 1.767962    | 0.294885 |
| 0.2   | -     | -         | -         | 0.330080      | 1.378959    | 0.607361 |
| 0.3   | -     | -         | -         | 0.279492      | 1.228859    | 0.928340 |
| 0.1   | 0.2   | -         | -         | 0.230683      | 2.218264    | 0.142164 |
| -     | 0.3   | -         | -         | 0.267124      | 2.489121    | 0.091084 |
| -     | 0.4   | -         | -         | 0.284107      | 2.588055    | 0.066514 |
| 0.1   | 0.1   | 0.05      | -         | 0.483377      | 2.578542    | 0.289614 |
| -     | -     | 0.1       | -         | 0.426808      | 2.554745    | 0.263534 |
| -     | -     | 0.15      | -         | 0.410630      | 2.530992    | 0.242355 |
| 0.1   | 0.1   | 0.03      | 0.1       | 0.277447      | 2.517484    | 0.358648 |
| -     | -     | -         | 0.2       | 0.481145      | 2.473393    | 0.330292 |
| -     | -     | -         | 0.3       | 0.633151      | 2.421493    | 0.311082 |

## Chapter 5

# CONCLUSION AND FUTURE WORK

Two difficulties have been examined in this thesis, the first being the review paper and the second being the extended work for it. Conclusion of both problems are as follows

### 5.1 Chapter 3

In the presence of an axial magnetic field the axisymmetric flow of a Maxwell fluid between two coaxially stretchable spinning disks with different angular velocities are discussed in this study. Heat transfer analysis is also examined by using the temperature-dependent thermal conductivity property. The dimensionless form of equations is obtained through Von Kármán similarity transformation. The flow, pressure, and temperature fields mechanisms have been depicted graphically and tabulatedly against the involved parameters.

- The presence of magnetic field is to reduce all three velocity components i.e axial, radial, azimuthal, which results in an increase in the fluid temperature.
- The Deborah number influence on axial and azimuthal velocities is seen to be diminishing in the absence of upper disk stretching.

- It is observed that the effect of Deborah number on axial and azimuthal velocities is shown to be diminishing.
- When both disks are stretched at the same rate, the Prandtl number reduces the temperature field.
- The magnetic field and thermal conductivity parameter raise the fluid temperature.

## 5.2 Chapter 4

In this chapter the Oldroyd-B nanofluid flow on a stretching and spinning disks using the Cattaneo-Christov heat flux is numerically examined. Fluid flow is studied in the existence of motile microorganism. Convective boundary conditions are employed on both the rotating disks. Suitable transformations are used to convert the governing partial differential equations (PDEs) for mass, momentum, heat, concentration and gyrotactic microorganisms equations into ordinary differential equations (ODEs). A numerical approach known as the BVP4c scheme used to solve these non-linear ODEs.

- The radial  $f'(\eta)$  and azimuthal  $g(\eta)$  velocity profiles is an increasing function of relaxation time parameter  $\beta_1$ .
- While the radial  $f'(\eta)$  and azimuthal  $g(\eta)$  velocity profiles is decreasing function of retardation time parameter  $\beta_2$ .
- The temperature rises as the Brownian motion parameter  $N_b$  and the Prandtl number  $Pr$  are increased.
- Fluid temperature increases for bottom disk Biot number  $\beta_{i1}$ , and reduces for upper disk Biot number  $\beta_{i2}$ .
- The Lewis number  $Le$  and Peclet number  $Pe$  enhance the concentration of microorganisms, but the Schmidt number  $Sc$  reduces.
- Concentration can be raised by using a less dispersed particle since diffusion forces fluid particles to travel from a highly concentrated location to a less concentrated one.

- Nusselt number reduces for the higher values of  $N_t$  and  $\beta_1$ , and increases for  $N_b$ , and  $\beta_2$ .

### 5.3 Future work

The present problem can be extended to the following models as well:

- The fluid flow may be extended to any other non-Newtonian fluid with appropriate boundary conditions.
- The model may be extended to homogeneous-heterogeneous reactions.
- The geometry can be changed.
- This problem can be solved for Prescribed surface temperature (PST) and Prescribed heat flux (PHF).
- The effect of the Darcy-Forchheimer and buoyancy effects may be added.

# Bibliography

- [1] Choi, S. U., & Eastman, J. A. Enhancing thermal conductivity of fluids with nanoparticles (No. ANL/MSD/CP-84938; CONF-951135-29). Argonne National Lab.(ANL), Argonne, IL (United States), (1995).
- [2] Buongiorno, J. Convective transport in nanofluids, (2006).
- [3] Kuznetsov, A. V., & Nield, D. A. Double-diffusive natural convective boundary-layer flow of a nanofluid past a vertical plate. *International Journal of Thermal Sciences*, 50(5) (2011) 712-717.
- [4] Ramzan, M., Riasat, S., Kadry, S., Long, C., Nam, Y., & Lu, D. Numerical simulation of 3D condensation nanofluid film flow with carbon nanotubes on an inclined rotating disk. *Applied Sciences*, 10(1) (2019) 168.
- [5] Dogonchi, A. S., & Ganji, D. D. Investigation of MHD nanofluid flow and heat transfer in a stretching/shrinking convergent/divergent channel considering thermal radiation. *Journal of Molecular Liquids*, 220 (2016) 592-603.
- [6] Udawattha, D. S., Narayana, M., & Wijayarathne, U. P. Predicting the effective viscosity of nanofluids based on the rheology of suspensions of solid particles. *Journal of King Saud University-Science*, 31(3) (2019) 412-426.
- [7] Hussanan, A., Salleh, M. Z., Khan, I., & Shafie, S. Convection heat transfer in micropolar nanofluids with oxide nanoparticles in water, kerosene and engine oil. *Journal of Molecular Liquids*, 229 (2017) 482-488.

- [8] Salari, S., & Jafari, S. M. Application of nanofluids for thermal processing of food products. *Trends in Food Science & Technology*, 97 (2020) 100-113.
- [9] Ayub, A., Sabir, Z., Shah, S. Z. H., Wahab, H. A., Sadat, R., & Ali, M. R. Effects of homogeneous-heterogeneous and Lorentz forces on 3-D radiative magnetized cross nanofluid using two rotating disks. *International Communications in Heat and Mass Transfer*, 130 (2022) 105778.
- [10] Waqas, H., Khan, S. A., Muhammad, T., & Yasmin, S. Convective heat transfer in magnetized flow of nanofluids between two rotating parallel disks. *International Journal of Chemical Reactor Engineering*, 20(4) (2022) 411-422.
- [11] Ghaffari, A., Muhammad, T., & Mustafa, I. Heat transfer enhancement in a power-law nanofluid flow between two rotating stretchable disks. *Pramana*, 96(1) (2022) 1-11.
- [12] Hussain, T., & Xu, H. Time-dependent squeezing bio-thermal MHD convection flow of a micropolar nanofluid between two parallel disks with multiple slip effects. *Case Studies in Thermal Engineering*, 31 (2022) 101850.
- [13] Naveen Kumar, R., Mallikarjuna, H. B., Tugalappa, N., Punith Gowda, R. J., & Umrao Sarwe, D. Carbon nanotubes suspended dusty nanofluid flow over stretching porous rotating disk with non-uniform heat source/sink. *International Journal for Computational Methods in Engineering Science and Mechanics*, 23(2) (2022) 119-128.
- [14] Maxwell, J. C. IV. On the dynamical theory of gases. *Philosophical transactions of the Royal Society of London*, (157) (1867) 49-88.
- [15] Bodnar, T., Pires, M., & Janela, J. Blood flow simulation using traceless variant of Johnson-Segalman viscoelastic model. *Mathematical Modelling of Natural Phenomena*, 9(6) (2014) 117-141.
- [16] Renardy, M., & Wang, X. Boundary layers for the upper convected Maxwell fluid. *Journal of Non-Newtonian Fluid Mechanics*, 189 (2012) 14-18.

- [17] Shateyi, S. A new numerical approach to MHD flow of a Maxwell fluid past a vertical stretching sheet in the presence of thermophoresis and chemical reaction. *Boundary Value Problems*, (1) (2013) 1-14.
- [18] Mustafa, M., Hayat, T., & Alsaedi, A. Rotating flow of Maxwell fluid with variable thermal conductivity: an application to non-Fourier heat flux theory. *International Journal of Heat and Mass Transfer*, 106 (2017) 142-148.
- [19] Hayat, T., Qayyum, S., Waqas, M., & Alsaedi, A. Thermally radiative stagnation point flow of Maxwell nanofluid due to unsteady convectively heated stretched surface. *Journal of molecular liquids*, 224 (2016) 801-810.
- [20] Prasannakumara, B. C. Numerical simulation of heat transport in Maxwell nanofluid flow over a stretching sheet considering magnetic dipole effect. *Partial Differential Equations in Applied Mathematics*, 4 (2021) 100064.
- [21] Hanif, H. A computational approach for boundary layer flow and heat transfer of fractional Maxwell fluid. *Mathematics and Computers in Simulation*, 191 (2022) 1-13.
- [22] Alsallami, S. A., Zahir, H., Muhammad, T., Hayat, A. U., Khan, M. R., & Ali, A. Numerical simulation of Marangoni Maxwell nanofluid flow with Arrhenius activation energy and entropy anatomization over a rotating disk. *Waves in Random and Complex Media*, (2022) 1-19.
- [23] Al Nuwairan, M., Hafeez, A., Khalid, A., & Syed, A. Heat generation/absorption effects on radiative stagnation point flow of Maxwell nanofluid by a rotating disk influenced by activation energy. *Case Studies in Thermal Engineering*, (2022) 102047.
- [24] Khan, R. M., Imran, N., Mehmood, Z., & Sohail, M. A Petrov–Galerkin finite element approach for the unsteady boundary layer upper-convected rotating Maxwell fluid flow and heat transfer analysis. *Waves in Random and Complex Media*, (2022) 1-18.
- [25] Oldroyd, J. G. On the formulation of rheological equations of state. *Proceedings of the Royal Society of London. Series A. Mathematical and Physical Sciences*, 200(1063) (1950) 523-541.



- [26] Irfan, M., Khan, M., Gulzar, M. M., & Khan, W. A. Chemically reactive and nonlinear radiative heat flux in mixed convection flow of Oldroyd-B nanofluid. *Applied Nanoscience*, 10(8) (2020) 3133-3141.
- [27] Khan, S. U., Rauf, A., Shehzad, S. A., Abbas, Z., & Javed, T. Study of bioconvection flow in Oldroyd-B nanofluid with motile organisms and effective Prandtl approach. *Physica A: Statistical Mechanics and its Applications*, 527 (2019) 121179.
- [28] Abbas, S. Z., Khan, W. A., Waqas, M., Irfan, M., & Asghar, Z. Exploring the features for flow of Oldroyd-B liquid film subjected to rotating disk with homogeneous/heterogeneous processes. *Computer Methods and Programs in Biomedicine*, 189, (2020) 105323.
- [29] Hafeez, A., Khan, M., & Ahmed, J. Stagnation point flow of radiative Oldroyd-B nanofluid over a rotating disk. *Computer Methods and Programs in Biomedicine*. 191 (2020) 105342.
- [30] Anwar, T., Khan, I., Kumam, P., & Watthayu, W. Impacts of thermal radiation and heat consumption/generation on unsteady MHD convection flow of an Oldroyd-B fluid with ramped velocity and temperature in a generalized darcy medium. *Mathematics*. 8(1) (2020) 130.
- [31] Ye, Z. Global regularity of the high-dimensional Oldroyd-B model in the corotational case. *Journal of Mathematical Analysis and Applications*, 486(2) (2020) 123867.
- [32] Ersoy, H. V. MHD flow of an Oldroyd-B fluid between eccentric rotating disks. *International Journal of Engineering Science*, 37(15) (1999) 1973-1984.
- [33] Bhatnagar, R. K., & Perera, M. G. N. Numerical solutions for flow of an Oldroyd fluid confined between coaxial rotating disks. *Journal of Rheology*, 26(1) (1982) 19-41.
- [34] Sajid, M., Abbas, Z., Javed, T., & Ali, N. Boundary layer flow of an Oldroyd-B fluid in the region of a stagnation point over a stretching sheet. *Canadian Journal of Physics*, 88(9) (2010) 635-640.
- [35] Hafeez, A., Khan, M., Ahmed, A., & Ahmed, J. Features of Cattaneo-Christov double diffusion theory on the flow of non-Newtonian Oldroyd-B nanofluid with Joule heating. *Applied Nanoscience*, 12(3) (2022) 265-272.

- [36] Wang, Y., Kumar, R. N., Gouadria, S., Helmi, M. M., Gowda, R. P., El-Zahar, E. R., & Khan, M. I. A three-dimensional flow of an Oldroyd-B liquid with magnetic field and radiation effects: An application of thermophoretic particle deposition. *International Communications in Heat and Mass Transfer*, 134 (2022) 106007.
- [37] Gangadhar, K., Kumari, M. A., Venkata Subba Rao, M., & Chamkha, A. J. Oldroyd-B nanoliquid flow through a triple stratified medium submerged with gyrotactic bioconvection and nonlinear radiations. *Arabian Journal for Science and Engineering*, (2022) 1-13.
- [38] Khan, M., Hafeez, A., & Ahmed, J. Von Karman swirling flow of an Oldroyd-B nanofluid with the influence of activation energy. *Mathematical Methods in the Applied Sciences*, 45(8) (2022) 4202-4209.
- [39] Pearson, C. E. Numerical solutions for the time-dependent viscous flow between two rotating coaxial disks. *Journal of Fluid Mechanics*, 21(4) (1965) 623-633.
- [40] Arora, R. C., & Stokes, V. K. On the heat transfer between two rotating disks. *International Journal of Heat and Mass Transfer*, 15(11) (1972) 2119-2132.
- [41] Turkyilmazoglu, M. Fluid flow and heat transfer over a rotating and vertically moving disk. *Physics of Fluids*, 30(6) (2018) 063605.
- [42] Turkyilmazoglu, M. Effects of uniform radial electric field on the MHD heat and fluid flow due to a rotating disk. *International Journal of Engineering Science*, 51 (2012) 233-240.
- [43] Khan, N. S., Shah, Q., Bhaumik, A., Kumam, P., Thounthong, P., & Amiri, I. Entropy generation in bioconvection nanofluid flow between two stretchable rotating disks. *Scientific reports*, 10(1) (2020) 1-26.
- [44] Bilal, S., Tassaddiq, A., Majeed, A. H., Nisar, K. S., Ali, F., & Malik, M. Y. Computational and physical examination about the aspects of fluid flow between two coaxially rotated disks by capitalizing non-Fourier heat flux theory: finite difference approach. *Frontiers in Physics*, 7 (2020) 209.

- [45] Lin, P., & Ghaffari, A. Steady flow and heat transfer of the power-law fluid between two stretchable rotating disks with non-uniform heat source/sink. *Journal of Thermal Analysis and Calorimetry*, 146(4) (2021) 1735-1749.
- [46] Ayub, A., Sabir, Z., Shah, S. Z. H., Wahab, H. A., Sadat, R., & Ali, M. R. Effects of homogeneous-heterogeneous and Lorentz forces on 3-D radiative magnetized cross nanofluid using two rotating disks. *International Communications in Heat and Mass Transfer*, 130 (2022) 105778.
- [47] Zeb, H., Wahab, H. A., Khan, U., Ehab, M., & Malik, M. Y. The Modified Heat Flux Modeling in Nanoparticles (Fe<sub>3</sub>O<sub>4</sub> and Aggregation Nanoparticle) Based Fluid between Two Rotating Disks. *Energies*, 15(11) (2022) 4088.
- [48] Mehdi, I., Abbas, Z., & Hasnain, J. MHD flow and heat transfer between two rotating disks under the effects of nanomaterials (MoS<sub>2</sub>) and thermal radiation. *Case Studies in Thermal Engineering*, 33 (2022) 101968.
- [49] Sharma, K., Kumar, S., Narwal, A., Mebarek-Oudina, F., & Animasaun, I. L. Convective MHD Fluid flow over Stretchable Rotating Disks with Dufour and Soret Effects. *International Journal of Applied and Computational Mathematics*, 8(4) (2022) 1-12.
- [50] Waqas, H., Khan, S. A., Muhammad, T., & Yasmin, S. Convective heat transfer in magnetized flow of nanofluids between two rotating parallel disks. *International Journal of Chemical Reactor Engineering*, 20(4) (2022) 411-422.
- [51] Alfvén, H. Existence of electromagnetic-hydrodynamic waves. *Nature*, 150(3805) (1942) 405-406.
- [52] Rashidi, S., Esfahani, J. A., & Maskaniyan, M. Applications of magnetohydrodynamics in biological systems-a review on the numerical studies. *Journal of Magnetism and Magnetic Materials*, 439 (2017) 358-372.
- [53] Hsu, J. P., Kao, C. Y., Tseng, S., & Chen, C. J. Electrokinetic flow through an elliptical microchannel: effects of aspect ratio and electrical boundary conditions. *Journal of Colloid and Interface Science*, 248(1) (2002) 176-184.

- [54] Turkyilmazoglu, M. Flow and heat over a rotating disk subject to a uniform horizontal magnetic field. *Zeitschrift für Naturforschung A*, 77(4) (2022) 329-337.
- [55] Hayes, M. A., & Ewing, A. G. Electroosmotic flow control and monitoring with an applied radial voltage for capillary zone electrophoresis. *Analytical Chemistry*, 64(5) (1992) 512-516.
- [56] Devi, S. A., & Devi, R. U. On hydromagnetic flow due to a rotating disk with radiation effects. *Nonlinear Analysis: Modelling and Control*, 16(1) (2011) 17-29.
- [57] Abbas, N., Malik, M. Y., & Nadeem, S. Stagnation flow of hybrid nanoparticles with MHD and slip effects. *Heat Transfer—Asian Research*, 49(1) (2020) 180-196.
- [58] Khatsayuk, M., Timofeev, V. & Demidovich, V. Numerical simulation and verification of MHD-vortex. *COMPEL-The international journal for computation and mathematics in electrical and electronic engineering*, 2020.
- [59] Platt, J. R. " Bioconvection patterns" in cultures of free-swimming organisms. *Science*, 133(3466) (1961) 1766-1767.
- [60] Kessler, J. O. Hydrodynamic focusing of motile algal cells. *Nature*, 313(5999) (1985) 218-220.
- [61] Basha, H. T., & Sivaraaj, R. Numerical simulation of blood nanofluid flow over three different geometries by means of gyrotactic microorganisms: Applications to the flow in a circulatory system. *Proceedings of the Institution of Mechanical Engineers, Part C: Journal of Mechanical Engineering Science*, 235(2) (2021) 441-460.
- [62] Hussain, T., & Xu, H. Time-dependent squeezing bio-thermal MHD convection flow of a micropolar nanofluid between two parallel disks with multiple slip effects. *Case Studies in Thermal Engineering*, 31 (2022) 101850.
- [63] Li, J. J., Xu, H., Raees, A., & Zhao, Q. K. Unsteady mixed bioconvection flow of a nanofluid between two contracting or expanding rotating discs. *Zeitschrift für Naturforschung A*, 71(3) (2016) 261-272.

- [64] Shehzad, S. A., Reddy, M. G., Rauf, A., & Abbas, Z. Bioconvection of Maxwell nanofluid under the influence of double diffusive Cattaneo–Christov theories over isolated rotating disk. *Physica Scripta*, 95(4) (2020) 045207.
- [65] Zuhra, S., Khan, N. S., Shah, Z., Islam, S., & Bonyah, E. Simulation of bioconvection in the suspension of second grade nanofluid containing nanoparticles and gyrotactic microorganisms. *AIP Advances*, 8(10) (2018) 105210.
- [66] Lance, G. N., & Rogers, M. H. The axially symmetric flow of a viscous fluid between two infinite rotating disks. *Proceedings of the Royal Society of London. Series A. Mathematical and Physical Sciences*, 266(1324) (1962) 109-121.
- [67] Turkyilmazoglu, M. Flow and heat simultaneously induced by two stretchable rotating disks. *Physics of Fluids*, 28(4) (2016) 043601.

18%  
SIMILARITY INDEX

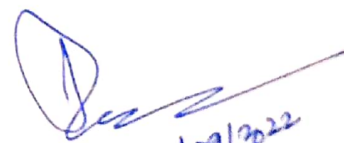
9%  
INTERNET SOURCES

14%  
PUBLICATIONS

6%  
STUDENT PAPERS

PRIMARY SOURCES

- 1 Submitted to Higher Education Commission Pakistan  
Student Paper 3%
- 2 Jawad Ahmed, Masood Khan, Latif Ahmad. "MHD swirling flow and heat transfer in Maxwell fluid driven by two coaxially rotating disks with variable thermal conductivity", Chinese Journal of Physics, 2019  
Publication 1%
- 3 Abdul Hafeez, Masood Khan, Jawad Ahmed. "Flow of magnetized Oldroyd-B nanofluid over a rotating disk", Applied Nanoscience, 2020  
Publication 1%
- 4 www.nature.com  
Internet Source 1%
- 5 Ali Ahmadian, Muhammad Bilal, Muhammad Altaf Khan, Muhammad Imran Asjad. "The non-Newtonian maxwell nanofluid flow between two parallel rotating disks under the effects of magnetic field", Scientific Reports, 2020 1%

  
29/09/2022